Transient three-pulse four-wave mixing spectra of magnetoexcitons coupled with an incompressible quantum liquid

M. E. Karadimitriou, E. G. Kavousanaki,* and I. E. Perakis
Department of Physics, University of Crete, Heraklion, Crete 71003, Greece and Institute of Electronic Structure & Laser, Foundation for Research and Technology-Hellas, Heraklion, Crete 71110, Greece

Keshav M. Dani
Center for Integrated Nanotechnologies, Los Alamos National Laboratory, Los Alamos, New Mexico 87545, USA
(Received 1 April 2010; revised manuscript received 14 August 2010; published 8 October 2010)

We present a nonequilibrium many-body formulation of the coherent ultrafast nonlinear optical response of doped semiconductors and systems with a strongly correlated ground state, such as the quantum Hall system (QHS). Our theory is based on a truncation of the density-matrix equations of motion in the absence of a small interaction parameter, obtained by expanding in terms of the optical field and by using Hubbard operator density matrices to describe the exact dynamics within a subspace of many-body states. We identify signatures of noninstantaneous interactions between magnetoexcitons (X) and the incompressible two-dimensional electron gas (2DEG) during femtosecond and picosecond time scales by describing X coupling to inter-Landau-level magnetoroton (MR) and magnetoplasmon excitations. We show that strong X coupling to X+MR configurations changes the temporal evolution of the nonlinear optical spectra as compared to the random-phase approximation (RPA). We calculate the three-pulse four-wave mixing signal, whose dependence on frequency and two time delays reflects the dephasing and relaxation of the strongly coupled X-2DEG system, and demonstrate that the dynamics of the X-2DEG interaction process can be resolved with femtosecond optical pulses. Our results shed light into unexplored subpicosecond and coherent dynamics of the QHS and may be used to interpret and guide two-dimensional correlation spectroscopy experiments.

DOI: 10.1103/PhysRevB.82.165313 PACS number(s): 42.50.Md, 73.43.Lp, 82.53.Mj, 78.20.Bh

I. INTRODUCTION

While the thermodynamic, linear response, and transport properties of many condensed-matter systems do not depend critically on the residual interactions among their elementary excitations, these interactions dominate the nonlinear response to external stimuli. The interactions among quasiparticles lead to decoherence and dephasing but also create new quantum coherences between many-body states.[1–4] Understanding and manipulating coherent dynamics is essential for building a new generation of controllable devices, whose speed limits are governed by the time scales of fundamental many-body processes. At the same time, a detailed understanding of the interaction processes leading to coherence and decoherence is of primary importance in the fields of macroscopic quantum phenomena, coherent control of molecular phenomena and femtochemistry, and for understanding the concepts underlying quantum information technology.[5]

In undoped semiconductors, the interactions among exciton quasiparticles determine the transient nonlinear optical response during the femtosecond temporal regime following photoexcitation,[1,3,6] where well-established quasiequilibrium concepts such as the free energy break down. To extract information from the experiments, nonequilibrium many-body theories such as the semiconductor Bloch equations,[4,7] dynamics controlled truncation scheme (DCTS),[2,8,9] correlation expansion,[3] Keldysh Green's functions,[4,7] and the canonical transformation "dressed semiconductor" approach[10] have been used. The exciton-exciton (X-X) interactions dominate the one-dimensional two-pulse four-wave mixing (FWM) spectra for negative time delays, where the phase-space filling (Pauli blocking, PSF) nonlinearities do not contribute.[1,6] The time-dependent Hartree-Fock treatment of the X-X interactions[4,7] predicts a negative time delay signal that decays twice as fast as the positive time delay signal.[1,6] In undoped semiconductors, deviations from such an asymmetric temporal profile were interpreted as a signature of correlations and scattering among exciton quasiparticles.[1,11]

To interpret the nonlinear optical spectra of undoped semiconductors, one need not take into account correlations involving ground-state electrons. A rigid Hartree-Fock ground state, with full valence band and empty conduction band, suffices when Auger processes are negligible.[12] The lowest electronic excitations are then *high-energy* interband transitions, which react instantaneously to the photoexcited carriers. In doped semiconductors and metals, however, the situation is different because *low-energy* electronic excitations interact with the photoexcited carriers. The fundamental reaction time, the period of one oscillation of the lowest excited state, can be long, in which case the system responds *unadiabatically* to photoexcitation. The nonlinear response is then strongly influenced by the quantum dynamics of the entire system, including the ground-state electrons. The theories describing the nonlinear response of undoped semiconductors must be extended when considering doped semiconductors with strong e-h correlations[10,13,14] or the quantum Hall system (QHS).[15–19] For example, the DCTS truncates the hierarchy of density matrices generated by the interactions based on the assumption that all Coulomb interactions occur between photoexcited e-h pairs and are thus dynamically generated by the optical excitation. In the QHS how-

ever, the standard diagrammatic expansions and DCTS factorizations, which assume a Hartree-Fock reference state and the absence of free ground-state carriers, break down. One may expect that the strong ground-state correlations lead to quantum dynamics triggered by photoexcitation.

The quantum well confinement along the z direction and the magnetic field quasiconfinement within the x-y plane discretizes the eigenstates of the QHS into *highly degenerate* discrete Landau levels (LLs). In the ground state, these LLs are partially filled with the correlated two-dimensional electron gas (2DEG).[20] The ratio of occupied states to LL degeneracy defines the filling factor ν. The LL degeneracy increases with magnetic field and above a threshold value, $\nu \leq 2$, the ground-state electrons only occupy the lowest LL (LL0) states; all the higher LLs (LL1,…) are then empty in the ground state. The coupling of the degenerate LL0 states by the Coulomb interaction results in a strongly correlated incompressible quantum liquid,[21] whose neutral collective charge excitations [magnetoplasmons (MPs) and magnetorotons (MRs),[20,22–27] excitons of composite fermions,[28–30] interband quasiexcitons,[31] etc.] depend on ν. For $\nu=1/m$, where m is an integer, the exchange Coulomb interactions can stabilize a ground state with polarized electron spins and charge excitation gap, the quantum Hall ferromagnet.[22,32–37] The interband optical properties of the QHS at fractional ν have mainly been studied so far with photoluminescence.[38] The fundamental interband excitations correspond to excitons and trions, i.e., charged excitons bound to a 2DEG electron, whose correlations and coupling with the 2DEG can be controlled experimentally by changing the asymmetry (doping profile) and width of the quantum well that determine the electron-hole separation.[31,39–43]

The study of the ultrafast nonlinear optical response of the QHS transcends across the boundaries of two largely disconnected communities. The nonlinear optical response is determined by an ensemble of n-h many-body states describing n photoexcited valence-band holes interacting with N_e+n conduction-band electrons, where N_e is the number of electrons in the ground state. In the absence of Auger processes, the nonlinear response to $(2\ell-1)$th order in the optical field only depends on few hole states, $n \leq \ell$. One could draw an analogy with the exciton+phonon states that determine the nonlinear response in undoped semiconductors[2,3] and consider products of up to ℓ e-h pairs with any number of 2DEG excitations. However, there are some important differences. In the QHS, both the X and 2DEG excitations are electronic in nature and therefore subject to Pauli and Coulomb correlations among each other. In contrast, in the undoped system, the X operators commute with the phonon operators. Additionally, in the QHS, the conduction band is partly occupied in the ground state with a correlated 2DEG while in the undoped system it is empty. As a result, the optical response of the QHS depends on the dynamics of an incompressible quantum liquid (2DEG), which responds to the photoexcited X's via the Coulomb interaction. Depending on ν, this dynamics is governed by Laughlin[21] and composite fermion[29,30] correlations. Finally, the photoexcited X can bind with a 2DEG electron, forming trion states with binding energies of a few millielectron volts that manifest themselves as extra peaks in the optical spectra.[31,39–43]

When the characteristic Coulomb energy exceeds the LL broadening due to disorder, the QHS ground state at $\nu=1$ corresponds to a ferromagnet with 100% spin polarization.[37] Neglecting small effects from LL mixing, this state is a single Slater determinant, represented exactly by Laughlin's wave function, with all LL0 spin-$\uparrow$ states full and all spin-$\downarrow$ states empty. For weak disorder, the ground state around $\nu=1$ includes a small population ($\propto|\nu-1|$) of topologically charged spin texture quasiparticles (skyrmions).[33–37] For larger disorder, the ground state is maximally spin polarized, however the empty states with respect to the $\nu=1$ ferromagnetic state are populated by conventional Laughlin quasiparticles. For strong disorder, the ferromagnetic order is destroyed.[37]

At fractional ν, the e-e interaction removes the degeneracy of the noninteracting system, producing robust ground states separated from the excited states by an energy gap. This nonperturbative effect can be interpreted by considering the formation of composite fermion quasiparticles, i.e., topological bound states of an electron and an even number of magnetic-flux quantized vortices.[29,30] The Coulomb interaction transforms the strongly interacting electrons into weakly interacting composite fermions. The partly filled lowest electron LL splits into several composite fermion LLs. Fractional quantum Hall effects then occur for integer composite fermion LL filling factors, when an integer number of composite fermion LLs are fully occupied.[29,30]

In this paper we present in full detail a microscopic many-body formulation of the ultrafast nonlinear optical response of a doped system with correlated ground state, which can be used to obtain the three-pulse ultrafast nonlinear optical spectra. The development of this theory was motivated by FWM experiments[16,18,44–49] demonstrating that, at low intensities, the 2DEG interactions change the spectral and temporal profile of the FWM signal in a significant way[45–47] as compared to a similar undoped quantum well.[50]

Our goal here is twofold. In the first part of the paper we obtain the third-order ultrafast nonlinear optical response for any filling factor by considering a hierarchy of density-matrix equations of motion. To truncate this hierarchy, we note that, in the QHS system, there is no small interaction parameter, except for the ratio of the Coulomb energy to the cyclotron energy that separates LLs in the large magnetic field limit (which however is comparable to 1 for magnetic fields up to 10 T where FWM experiments are performed). In the absence of a small parameter, we obtain a closed system of Hubbard operator density-matrix equations of motion that describes the exact dynamics, within a subspace of 0-h, 1-h, and 2-h many-body states, including relaxation. Hubbard operator equations of motion have been used before to study the dynamics of the Hubbard Hamiltonian,[51] the spin excitations in the manganites,[52] X-X correlations in the nonlinear response of undoped semiconductors,[53] and the linear response of quantum liquids.[26,27,31,43,54]

Our scheme proceeds in two steps. First we obtain the linear interband coherent amplitudes (e.g., the optical polarization), by calculating the time evolution of the 1-h photoexcited many-body state within an appropriate subspace of 1-h+(N_e+1)-e states that include excited 2DEG configurations (as, e.g., in Refs. 14 and 31). This step treats the cor-

relations of the photoexcited e-h pair with the ground state 2DEG, which lead, e.g., to the formation of trion bound states, quasiexcitons, or a strong 2DEG perturbation due to shake up of electronic excitations (dynamical 2DEG response). As a second step, we treat the nonlinear contributions to the intraband and interband density matrices by adopting an expansion in terms of the optical field and noting that, similar to the DCTS,[2] there is a one to one correspondence between number of valence holes and number of emitted/absorbed photons. This correspondence allows us to treat separately the dynamics within subspaces of many-body states with fixed (small) number of holes. In the undoped system, $N_e=0$ and the only carriers present in the system come from e-h pairs generated by the optical excitation. As a result, the 1-h and 2-h subspaces are spanned by X and $X+X$ states, which reduces the number of independent density matrices as in the DCTS.[2,8,9]

Given the complexity of describing the full dynamics within the 2-h+(N_e+2)-e subspace and the need to include incoherent effects due to relaxation,[2,9] we introduce a decomposition of the time-evolved many-body wave function into correlated and uncorrelated parts, analogous to the cumulant expansions of the DCTS, which however applies to systems with a populated correlated ground state. This decomposition allows us to separate the contributions to the interaction-induced nonlinear density matrices that can be expressed as products of interband coherent amplitudes (polarizations) from fully correlated contributions, whose dynamics differs due to multiparticle correlations among photoexcited carriers leading to memory effects.[1,9,11] Our formulation applies to any strongly correlated system under the following general conditions: (i) an expansion in terms of the optical field is appropriate, (ii) the optical response is determined by electronic transitions between two or more "bands," i.e., many-body states consisting of different atomic orbitals, which are disconnected to good approximation in the absence of photoexcitation, and (iii) the optical transitions occur between a band that is either completely filled or completely empty in the unexcited system and a band that is partially filled.

In the second part of the paper, we apply the above theory to identify the main qualitative temporal and spectral features of the three-pulse FWM signal arising from X coupling to LL0$\rightarrow$LL1 inter-LL magnetoroton excitations. This particular calculation was motivated by the experiments of Chemla and co-workers,[16,18,44–49] who observed an unusual FWM spectral and temporal profile for $\nu<2$ when exciting close to LL1 and looking at LL0 energies. Since the photoexcitation of the LL0 resonance did not produce any unusual behavior for the mobilities of their symmetrically doped quantum wells, we suppress any trion effects here by using the ideal 2D system Hamiltonian at $\nu=1$ and assume a small ratio of Coulomb-to-cyclotron energy to highlight light-induced dynamical inter-LL coupling nonlinear effects in the presence of an incompressible 2DEG.

Some aspects of our theory may be found in Refs. 15–19, which focused on the initial coherent temporal regime. There, a qualitative understanding of the main experimental features[45–47] was obtained by solving a simple average polarization model. This model was derived from the theory of Ref. 15 by using a Lanczos basis of three many-body states, with interaction parameters obtained by fitting the experiment. Here we derive the exact third-order nonlinear optical response, including nonlinearities neglected in our earlier work, and also address the incoherent temporal regime following the decay of the interband polarization, ignored in our earlier works. In addition to describing microscopically the coherent temporal oscillations and their interaction-induced decay, we identify a FWM signal that rises on a picosecond time scale and reflects the gradual buildup of populations of X+MP and X+MR configurations, as a result of X-2DEG interactions. Our quantum kinetic calculation uses a continuum basis of many-body states, unlike for our average polarization model.[18,19] They allow us to identify, in the simplest possible way, experimental signatures due to magnetoroton 2DEG excitations, which result from many-body corrections to the local field of an incompressible quantum liquid. These excitations are missed by the random-phase approximation (RPA) treatment of the 2DEG interactions, which only gives MPs.[25–27]

The outline of this paper is as follows. In Sec. II we discuss the many-body Hamiltonian and the collective operators that create the electronic excitations. In Sec. III we discuss the interaction effects that present the main challenge for describing the optical dynamics. In Sec. IV we present an exact formulation of the QHS linear absorption valid for any ν. In Sec. V we obtain the second-order intraband density matrices that describe photoexcited populations and intraband coherences. In Sec. VI we obtain the third-order interband density matrices and describe the different interaction-induced contributions to the nonlinear polarization that gives the transient nonlinear optical spectra. In Sec. VII we use the above formulation to calculate the linear absorption and the three-pulse transient FWM spectra at $\nu=1$, as function of frequency and two time delays. We end with our conclusions. Some technical details are presented in four appendices.

II. HAMILTONIAN AND COLLECTIVE EXCITATIONS

The general second-quantization Hamiltonian describing the system in the absence of optical fields reads

$$H=\sum_{\alpha}(E_g+\varepsilon_{\alpha}^{c})\hat{e}_{\alpha}^{\dagger}\hat{e}_{\alpha}+\sum_{\alpha}\varepsilon_{\alpha}^{v}\hat{h}_{\alpha}^{\dagger}\hat{h}_{\alpha}+H_{int}, \tag{1}$$

where $\hat{e}_{\alpha}^{\dagger}$ ($\hat{h}_{\alpha}^{\dagger}$) create a conduction (valence) electron (hole) state in a state labeled by a composite index α that contains all relevant single-particle quantum numbers, $\varepsilon_{\alpha}^{e,h}$ are the discrete LL energies, and E_g is the semiconductor band gap. H_{int} describes the e-e, e-h, and h-h Coulomb interactions,

$$\begin{aligned}H_{int}=\frac{1}{2}\sum_{\alpha_1\alpha_2\alpha_3\alpha_4}[&v^{ee}_{\alpha_1\alpha_2,\alpha_3\alpha_4}\hat{e}^{\dagger}_{\alpha_3}\hat{e}^{\dagger}_{\alpha_1}\hat{e}_{\alpha_2}\hat{e}_{\alpha_4}\\&+v^{hh}_{\alpha_1\alpha_2,\alpha_3\alpha_4}\hat{h}^{\dagger}_{\alpha_3}\hat{h}^{\dagger}_{\alpha_1}\hat{h}_{\alpha_2}\hat{h}_{\alpha_4}-v^{eh}_{\alpha_1\alpha_2,\alpha_3\alpha_4}\hat{h}^{\dagger}_{\alpha_3}\hat{e}^{\dagger}_{\alpha_1}\hat{e}_{\alpha_2}\hat{h}_{\alpha_4}\\&-v^{he}_{\alpha_1\alpha_2,\alpha_3\alpha_4}\hat{e}^{\dagger}_{\alpha_3}\hat{h}^{\dagger}_{\alpha_1}\hat{h}_{\alpha_2}\hat{e}_{\alpha_4}].\end{aligned} \tag{2}$$

By treating the coupling of the optical field $E(t)$ within the dipole approximation,[7] the total Hamiltonian reads

$$H(t) = H - [d(t)\hat{X}^\dagger + \text{H.c.}], \tag{3}$$

where $d(t)=\mu E(t)$ is the Rabi energy, μ is the interband transition matrix element, and $\hat{X}^\dagger$ is the interband transition operator, expressed as a linear combination of e-h creation operators $\hat{e}_\alpha^\dagger \hat{h}_\beta^\dagger$.

To demonstrate the generic qualitative features due to the nonequilibrium correlations, one can adopt a simple two-band Hamiltonian H describing two-dimensional electrons and holes subject to a perpendicular magnetic field.[4,7] We also consider for simplicity right-circularly (σ_+) polarized light, which gives a single LL0 absorption peak via a single interband transition that creates spin-$\downarrow$ electrons, and simplifies the interpretation of the experiments.[47] In the Landau gauge, $\alpha=(k,n,\sigma)$, where k is proportional to the cyclotron orbit center x coordinate, n is the LL index, and s denotes the spin. $\varepsilon_\alpha^{e,h}=\omega_c^{e,h}(n+1/2)$, where $\omega_c^{e,h}=eB/m_{e,h}$ are the electron and hole cyclotron energies ($\hbar=1$). The interaction matrix elements are given in Appendix A. Although the discrete energy LLs resemble an atomic system, they have a macroscopic degeneracy $N=L^2/2\pi\ell^2$, where L is the system size and l is the magnetic length. We introduce the LL filling factor $\nu=N_e/N=2\pi\ell^2 n_e$, where N_e (n_e) denotes the number (density) of electrons in the ground state.

Some particularities of the realistic system, such as finite quantum well height and width, doping and confining potential profile, spin-orbit interaction, disorder effects, etc., are important for comparing to experiment.[43] For example, the optical selection rules resulting from invariance under magnetic translations (geometric symmetry),[55] particle-hole symmetry between conduction electrons and valence holes (hidden symmetry),[39,56,57] and the absence of disorder in the ideal 2D system are partially lifted in the realistic system. The formalism developed in the first part of this paper also applies to the realistic system.

The optical dynamics is determined by interband and intraband excitations of the ground state $|G\rangle$. In the undoped system, the following operators create {1-LLn-e+1-LLm-h} excitons with total momentum $\mathbf{q}$:

$$\hat{X}_{\mathbf{q}nm}^\dagger = \frac{1}{\sqrt{N}}\sum_k e^{ikq_x\ell^2}\hat{e}_{k+q_y/2n\downarrow}^\dagger \hat{h}_{-k+q_y/2m\downarrow}^\dagger. \tag{4}$$

In the ideal system, the selection rules allow the direct photoexcitation of $\mathbf{q}=0$, $m=n$ e-h pairs, created by $\hat{X}_n^\dagger=\hat{X}_{\mathbf{q}=0nn}^\dagger$. The Pauli exchange effects between such X's are described by the deviation of their commutator from bosonic behavior,

$$[\hat{X}_n,\hat{X}_m^\dagger] = \delta_{nm}(1-\hat{\nu}_{nm}), \tag{5}$$

where $\hat{\nu}_{nm}=\hat{\nu}_{nm}^e+\hat{\nu}_{nm}^h$. The operators

$$\hat{\nu}_{nm}^h = \frac{1}{N}\sum_k \hat{h}_{-kn\downarrow}^\dagger \hat{h}_{-km\downarrow}, \quad \hat{\nu}_{nm}^e = \frac{1}{N}\sum_k \hat{e}_{kn\downarrow}^\dagger \hat{e}_{km\downarrow} \tag{6}$$

describe the LLn filling factors ($n=m$), due to ground state or photoexcited carriers, and create inter-LL excitations ($n\neq m$). For the intraband excitations, we introduce the collective electron and hole excitation operators analogous to the magnetoexciton operators, Eq. (4),

$$\hat{\rho}_{\mathbf{q}nm\sigma}^e = \frac{1}{\sqrt{N}}\sum_k e^{iq_xk\ell^2}\hat{e}_{k+q_y/2n\sigma}^\dagger \hat{e}_{k-q_y/2m\sigma} \tag{7}$$

and

$$\hat{\rho}_{\mathbf{q}nm\sigma}^h = \frac{1}{\sqrt{N}}\sum_k e^{iq_xk\ell^2}\hat{h}_{-k+q_y/2n\sigma}^\dagger \hat{h}_{-k-q_y/2m\sigma}. \tag{8}$$

Similar to the collective excitations of quantum liquids,[54] the states $\hat{\rho}_{\mathbf{q}n'n\sigma}^e|G\rangle$ have been used as a basis to describe the neutral excitations of the Laughlin state at certain ν (single-mode approximation).[20,22,27,28] Within this approximation, the neutral collective charge excitations of the 2DEG correspond to MP modes created by $\hat{\rho}_{\mathbf{q}nm\sigma}^e$.[20,22,27,28] In contrast to phonons,[2] MP-MP and X-MP Pauli exchange effects are important and are described by the commutators in Appendix B. A LL$m\rightarrow$LLn MP can be considered as an "exciton" formed by a LLn electron and a hole in the LLm 2DEG. However, such excitons couple to the 2DEG electrons. Comparisons to small system exact diagonalizations showed that the single-mode approximation describes well the excitation energy dispersion for $\nu=1/(2m+1)$, where m is an integer, at small and intermediate wave vectors q close to the roton minimum. However, it does not work well for other ν or for large q. In this case, one can consider composite fermion quasielectron-quasihole excitations.[28,31] The collective 2DEG excitations at $\nu=n/(2mn+1)$, where n is an integer, are then described by acting with the operators [Eq. (7)] on the Slater determinant of n filled LLs, multiplying by the Jastrow factor, and then projecting to the lowest LL.[28] For $\nu=1/(2m+1)$, the two above approaches produce the same results for small q while for other ν they differ for all q.

Analogous to the above "2DEG exciton" states, we introduce the zero-momentum interband exciton states $|X_n\rangle=\hat{X}_{\mathbf{q}=0nn}^\dagger|G\rangle$. The difference from undoped semiconductors is that $\hat{X}_n^\dagger$ act on the strongly correlated ground state $|G\rangle$ of the Hamiltonian H with N_e electrons. Using Eq. (5), we obtain the orthogonality relation

$$\langle X_n|X_m\rangle = (1-\nu_n)\delta_{nm}, \tag{9}$$

where $\nu_n=\langle G|\hat{\nu}_{nn}^e|G\rangle$ is the ground-state filling factor of the LLn electron states. At $\nu=1$, excitons and quasiexcitons coincide. At fractional ν, exact diagonalization calculations at $\nu=1/3$ (Ref. 31) showed that the zero-momentum exciton and quasiexciton states give equivalent results when used to approximate the $q=0$ eigenstates.

III. INTERACTION EFFECTS

In this section we obtain equations of motion for the nonlinear polarization, in a form that establishes the connection with undoped semiconductor and atomic systems. We also use the ideal 2D system Hamiltonian to discuss the interaction effects in a system with hidden symmetry, which simplifies the optical response.[56]

We start by expanding the interband transition operator $\hat{X}$, which describes the coupling of the optical field in the Hamiltonian $H(t)$, in terms of e-h pair creation operators:

$\hat{X}^\dagger = \sqrt{N}\Sigma_n \hat{X}_n^\dagger$. In the ideal 2D system, where $\hat{X}^\dagger = \Sigma_{nk} \hat{e}_{kn}^\dagger \hat{h}_{-kn}^\dagger$, a natural choice are the zero-momentum LL exciton operators $\hat{X}_{\mathbf{q}=0nn}^\dagger$ due to the hidden symmetry.[56] However, in our discussion below $\hat{X}_n^\dagger$ can be any combination of e-h creation operators $\hat{e}_\alpha^\dagger \hat{h}_\beta^\dagger$.

Within the dipole approximation, the optical response is described by the polarization (e-h coherence)[4,6]

$$P(t) = \mu \sum_n P_n(t), \quad P_n(t) = \frac{\langle \hat{X}_n \rangle}{\sqrt{N}}, \tag{10}$$

whose equation of motion is obtained from Eq. (B1). In the doped system, this equation of motion depends on the interactions between the e-h pair X_n and the 2DEG thermal carriers, which can lead to a strong perturbation of the 2DEG.[14,31] Such X_n-2DEG interactions couple X_n with the X+2DEG* states $|Y_n\rangle$ (2DEG* denotes from now on an excited 2DEG configuration) defined by[15]

$$H|X_n\rangle = \Omega_n |X_n\rangle - (1-\nu_n) \sum_{m \neq n} V_{mn} |X_m\rangle + |Y_n\rangle \tag{11}$$

with the orthogonality requirement $\langle X_m | Y_n \rangle = 0$. The latter condition, together with Eq. (9), gives

$$\Omega_n = \frac{\langle X_n | H | X_n \rangle}{\langle X_n | X_n \rangle}, \quad V_{nn'} = -\frac{\langle X_n | H | X_{n'} \rangle}{(1-\nu_n)(1-\nu_{n'})} \tag{12}$$

for any strongly correlated ground state. It is then useful to introduce the operator

$$\hat{Y}_n = [\hat{X}_n, H] - \Omega_n \hat{X}_n + (1-\nu_n) \sum_{n' \neq n} V_{nn'} \hat{X}_{n'} \tag{13}$$

and obtain the equation of motion

$$i\partial_t P_n(t) - \Omega_n P_n(t) + (1-\nu_n) \sum_{n' \neq n} V_{nn'} P_{n'}(t) = -d(t)[1 - n_n(t)] + \frac{\langle \hat{Y}_n \rangle}{\sqrt{N}}. \tag{14}$$

Equation (11) subtracts the static and noninteracting contributions on the light-hand side of Eq. (14) and also defines the first step in a Lanczos computational approach to the time-dependent problem of the nonlinear optical response,[15] whose advantages have been discussed in the context of quantum chemistry.[58] The first term on the right-hand side (rhs) of Eq. (14) describes the PSF effects, determined by the time-dependent LLn filling factor

$$n_n(t) = \langle \hat{\nu}_{nn} \rangle, \quad \hat{\nu}_{nn} = \hat{\nu}_{nn}^e + \hat{\nu}_{nn}^h, \tag{15}$$

which describes the LLn ground state and photoexcited electron and hole populations [see Eq. (6)].

In the absence of interactions, $\hat{Y}_n = 0$ and Eq. (14) reduces to optical Bloch equations of an atomiclike system of discrete LLs. In the undoped system, $\langle \hat{Y}_n \rangle$ describes the interactions between X_n and the photoexcited carriers.[59] The understanding of the effect of the 2DEG and incompressible quantum liquid on $\langle \hat{Y}_n \rangle$ is the main goal of this paper. To elucidate this interaction-induced contribution, we consider the ideal 2D system and obtain after straightforward algebra by using Eqs. (C1) and (12),

$$\hat{Y}_n = \frac{1}{2\pi\ell^2\sqrt{N}} \sum_{\mathbf{q}m} v_q \hat{\rho}_{\mathbf{q}} [\phi_{nm}(-\mathbf{q}) \hat{X}_{\mathbf{q}mn} - (n \leftrightarrow m)] - \sum_m \left[\frac{\hat{X}_m}{1-\nu_m} \int \frac{d\mathbf{q}}{(2\pi)^2} v_q \phi_{mn}(\mathbf{q}) \langle G | \hat{\rho}_{-\mathbf{q}} \hat{\rho}_{\mathbf{q}mn\downarrow}^e | G \rangle - \frac{\hat{X}_n}{1-\nu_n} \int \frac{d\mathbf{q}}{(2\pi)^2} v_q \phi_{nm}(\mathbf{q}) \langle G | \hat{\rho}_{-\mathbf{q}} \hat{\rho}_{\mathbf{q}nm\downarrow}^e | G \rangle \right], \tag{16}$$

where we introduced the operator

$$\hat{\rho}_{\mathbf{q}} = \sum_{n'm'\sigma} [\phi_{m'n'}(\mathbf{q}) \hat{\rho}_{\mathbf{q}m'n'\sigma}^e - \phi_{n'm'}(\mathbf{q}) \hat{\rho}_{\mathbf{q}m'n'\sigma}^h]. \tag{17}$$

The second term on the rhs of Eq. (16) subtracts the noninteracting/static 2DEG contribution to the X energies and couplings, Eq. (12), determined by the ground-state static structure factor.[20,22] We note from Eq. (16) that, due to the hidden symmetry,[56,57] $\hat{Y}_n$ vanishes if we project to states in a given LL, $n=m$. Therefore, in the absence of LL mixing, the optical response of the ideal 2D system resembles that of an atomiclike system and X_n is approximately decoupled from the 2DEG.

In the general system, $\langle \hat{Y}_n \rangle$ can be expanded in terms of density matrices of the form $\langle \hat{e}^\dagger \hat{e} \hat{e} \hat{h} \rangle$ and $\langle \hat{h}^\dagger \hat{h} \hat{e} \hat{h} \rangle$, which describe the interaction of an e-h pair with an additional carrier. The factorization of such density matrices gives the semiconductor Bloch equations.[4,7,59] However, this Hartree-Fock approximation misses biexciton, trion, and X-2DEG inelastic scattering effects by assuming a static 2DEG. In the undoped system, where the conduction band is empty and the valence band is full, $\hat{Y}_n^\dagger |G\rangle = 0$ and Eq. (16) describes interactions among photoexcited carriers only. These can be treated similar to the DCTS by projecting to a subspace of X and X+X states.[60] In the QHS, Eq. (16) describes, in addition, X-2DEG interactions and the resulting dynamical 2DEG response. Such effects are described by considering the action of $\hat{Y}_n^\dagger$, or more generally operators of the form $\hat{e}^\dagger \hat{e}^\dagger \hat{h}^\dagger \hat{e}$, on the subspace of 0-$h$+$N_e$-$e$ states. For example, in the general system the state $\hat{Y}_n^\dagger |G\rangle$ is a linear combination of e-h pair+2DEG excitation states. Recalling that the operators $\hat{\rho}_{\mathbf{q}nm\sigma}^e$ create/annihilate the MPs, one can interpret $|Y_n\rangle$, Eq. (16), as a linear combination of the continuum of X+MP configurations that couple to X_n via the X-2DEG interaction. In the limit $N_e=1$, relevant for $\nu \ll 1$, $|Y_n\rangle$ describes one hole and two electrons in excited states unoccupied in the ground state, i.e., trion configurations, while in $|X_n\rangle$ one of the two electrons remains in its ground-state configuration. In the doped system, the strong interaction between a finite momentum exciton and the 2DEG can bind a 2DEG electron and form a trion state analogous to the $N_e=1$ case, which is correlated with a 2DEG hole. This is the case when the symmetry of the ideal 2D system is broken.[43] At fractional ν, the above trion effects occur between composite fermions, lead-

ing to quasiexcitons.[31] It is clear that, when calculating the optical response, given by $\langle \hat{X}_n \rangle$, in the doped system, the coupling to the density matrices $\langle \hat{Y}_n \rangle$ in Eq. (14) must be treated nonperturbatively.

We now turn to the populations n_n, Eq. (15), which are obtained from the equation of motion for $\langle [\hat{X}_n, \hat{X}_n^\dagger] \rangle$ and Eq. (5). Calculating the commutator $[H, [\hat{X}_n, \hat{X}_n^\dagger]]$ from Eq. (13) by using the property $[A,[B,C]]+[C,[A,B]]+[B,[C,A]]=0$ we obtain

$$\partial_t n_n(t) = 2\ \mathrm{Im}[2d^*(t)P_n(t) + \langle [\hat{Y}_n, \hat{X}_n^\dagger] \rangle^*] \tag{18}$$

with initial condition given by the ground-state filling factor ν_n. The first term on the rhs describes the photoexcitation process while the density matrix $\langle [\hat{Y}_n, \hat{X}_n^\dagger] \rangle$ describes the interaction effects on the population quantum kinetics, i.e., the redistribution of the photoexcited carriers among the LLs and the intraband coherences among the photoexcited many-body states. The corresponding physical processes become more clear by calculating the above commutator in the ideal 2D system using Eq. (16),

$$\begin{aligned}\langle [\hat{Y}_n, \hat{X}_n^\dagger] \rangle = & \frac{1}{2\pi l^2 N} \sum_{\mathbf{q}m'n'} v_q \langle [\phi_{n'n}(\mathbf{q}) \hat{X}^\dagger_{\mathbf{q}n'n} - \phi_{nn'}(\mathbf{q}) \hat{X}^\dagger_{\mathbf{q}nn'}] \\ & \times [\phi^*_{m'n}(\mathbf{q}) \hat{X}_{\mathbf{q}m'n} - \phi^*_{nm'}(\mathbf{q}) \hat{X}_{\mathbf{q}nm'}] \rangle \\ & - \frac{1}{2\pi l^2 N} \sum_{\mathbf{q},m' \neq n} v_q [\phi_{nm'}(\mathbf{q}) \Delta \langle \hat{\rho}_{-\mathbf{q}} \hat{\rho}^e_{\mathbf{q}nm'\downarrow} \rangle \\ & - \phi_{m'n}(\mathbf{q}) \langle \hat{\rho}_{-\mathbf{q}} \hat{\rho}^h_{\mathbf{q}nm'\downarrow} \rangle] \\ & - \frac{\Delta \langle \hat{\nu}_{nn} \rangle}{2\pi l^2 N (1-\nu_n)} \sum_{\mathbf{q},n''m''\sigma} \sum_{m' \neq n} v_q \phi_{nm'}(\mathbf{q}) \phi^*_{n''m''}(\mathbf{q}) \\ & \times \langle G | \hat{\rho}^e_{-\mathbf{q}m''n''\sigma} \hat{\rho}^e_{\mathbf{q}nm'\downarrow} | G \rangle, \end{aligned} \tag{19}$$

where $\Delta\langle \hat{O} \rangle = \langle \hat{O} \rangle - \langle G|\hat{O}|G \rangle$. The first term on the rhs of Eq. (19) is determined by the interactions of the X populations and $X \leftrightarrow X$ coherences $\langle \hat{X}^\dagger_{\mathbf{q}nm} \hat{X}_{\mathbf{q}n'm'} \rangle$, similar to the undoped system.[2] Analogous effects determine the second term, with additional contributions in the QHS due to the scattering of the photoexcited carriers with the thermal 2DEG. The last term is due to the ground-state correlations, described by the static 2DEG structure factor.

Equation (19) reduces the X-2DEG quantum kinetics to the calculation of the density matrices $\langle \hat{X}^\dagger \hat{X} \rangle$, $\langle \hat{\rho}^e_\sigma \hat{\rho}^e_\downarrow \rangle$, $\langle \hat{\rho}^e_\sigma \hat{\rho}^h_\downarrow \rangle$, and $\langle \hat{\rho}^h_\downarrow \hat{\rho}^h_\downarrow \rangle$. To second order in the optical field, only many-body states with a single valence hole contribute to such intraband density matrices (discussed in the next section). Thus, $\langle \hat{h}^\dagger \hat{h}^\dagger \hat{h} \hat{h} \rangle = O(E^4)$ and

$$\langle \hat{\rho}^h_{-\mathbf{q}m'n'\sigma} \hat{\rho}^h_{\mathbf{q}nm\sigma} \rangle = \delta_{\sigma\downarrow} \nu^h_{m'm} \delta_{nn'} + O(E^4). \tag{20}$$

This factorization of the density matrix $\langle \hat{\rho}^h \hat{\rho}^h \rangle$ is *exact* to $O(E^2)$. In the undoped system, the same holds true for the density matrices $\langle \hat{\rho}^e \hat{\rho}^e \rangle$ since only states with a single electron contribute to $O(E^2)$. In the QHS this is not true due to the ground-state electron populations. By substracting the factorizable contribution and noting that $\mathbf{q} \neq 0$ in Eq. (19), we obtain

$$\langle \hat{\rho}^e_{-\mathbf{q}m'n'\downarrow} \hat{\rho}^e_{\mathbf{q}nm\downarrow} \rangle = (\delta_{n,n'} - \nu^e_{nn'}) \nu^e_{m'm} + C^{m'n'}_{mn}(\mathbf{q}), \tag{21}$$

where we introduced the four-electron density matrix

$$\begin{aligned} C^{m'n'}_{mn}(\mathbf{q}) = & \nu^e_{nn'} \nu^e_{m'm} + \frac{1}{N} \sum_{kk'} e^{iq_x(k-k')\ell^2} \\ & \times \langle \hat{e}^\dagger_{k+q_y/2n\downarrow} \hat{e}^\dagger_{k'-q_y/2m'\downarrow} \hat{e}_{k'+q_y/2n'\downarrow} \hat{e}_{k-q_y/2m\downarrow} \rangle. \end{aligned} \tag{22}$$

In the undoped system, $C=0$ to $O(E^2)$ since it involves operators that annihilate two electrons. In the QHS, a finite $O(E^2)$ contribution can arise due to the scattering of spin-$\downarrow$ photoexcited and ground-state electrons. Similarly, the density matrices $\langle \hat{\rho}^e_\uparrow \hat{\rho}^e_\downarrow \rangle$ and $\langle \hat{\rho}^e_\uparrow \hat{\rho}^h_\downarrow \rangle$, which vanish to $O(E^2)$ in the undoped system, contribute in the QHS due to photoexcited carrier scattering with spin-$\uparrow$ ground-state electrons.

To establish the connection with the DCTS, we note when calculating $\nu^{e,h}_{nn'}$ that, to $O(E^2)$, in the undoped system the operators $\hat{\nu}^{e,h}_{nn'}$ act on states with a single e-h pair. One can thus multiply $\hat{\nu}^{e,h}_{nn'}$ by the h or e number operator and express the above density matrices in terms of $\langle \hat{X}^\dagger \hat{X} \rangle$. In the QHS, this is also possible in the case of spin-$\downarrow$ photoexcited electrons when the ground-state 2DEG is spin-$\uparrow$ polarized and $C=O(E^4)$.[61] The density matrices $\langle \hat{\rho}^e_\uparrow \hat{\rho}^e_\downarrow \rangle$ and $\langle \hat{\rho}^e_\uparrow \hat{\rho}^h_\downarrow \rangle$ can then be expressed in the form $\langle \hat{\rho}^e_\uparrow \hat{X}^\dagger \hat{X} \rangle$ (Ref. 17) and describe the coherent coupling of an X initial state to a final state consisting of an X plus an excitation of the spin-$\uparrow$ 2DEG. The equations of motion of the above independent density matrices require however the consideration of multiple 2DEG excitations,[14,31] discussed in the next section.

IV. LINEAR INTERBAND POLARIZATION

In this section we obtain P_n to $O(E)$, which determines the linear absorption spectrum. We note that the Hamiltonian H conserves the number of valence holes while in the ground state the valence band is full. As a result, the $O(E)$ contribution to P_n comes from 1-h+(N_e+1)-e states. We denote $|\psi_{1L}(t)\rangle$ the $O(E)$ 1-h contribution to the many-body state that evolves in time from the correlated ground state $|G\rangle$ according to the Hamiltonian $H(t)$, Eq. (3).[15,17] The $O(E)$ contribution to the interband density matrix $\langle \hat{Z} \rangle$, where $\hat{Z}$ is any operator that reduces the number of holes by one, is then given by

$$\langle \hat{Z} \rangle^L = \langle G|\hat{Z}|\psi_{1L}(t)\rangle = \langle\ |G\rangle\langle G|\hat{Z}|\ \rangle^L, \tag{23}$$

which coincides with the linearized density matrix of the Hubbard operator $|G\rangle\langle G|\hat{Z}|$.[53] We can thus reduce the calculation of $\langle \hat{Z} \rangle^L$ to a closed system of equations of motion of Hubbard operator density matrices $\langle |G\rangle\langle \alpha| \rangle$, where the states $|\alpha\rangle$ span the 1-h subspace of interest.

$|\psi_{1L}(t)\rangle$ evolves in time as follows:[15]

$$i\partial_t|\psi_{1L}\rangle = H|\psi_{1L}\rangle - d(t)\sum_n \langle X_n|\hat{X}^\dagger|G\rangle|X_n\rangle. \quad (24)$$

The Fermi's golden rule calculation of the linear absorption spectrum is recovered by expanding $|X_n\rangle$ in terms of the many-body eigenstates of H while the solution is trivial if $|X_n\rangle$ is an eigenstate of H. However, $|X_n\rangle$ is not an eigenstate of H, so the time evolution leads to the static couplings $V_{nn'}$, Eq. (12), in both doped and undoped systems[59] and to the coupling to "trion" configurations, Eq. (11). In the doped system, the nontrivial problem is to describe the dynamical 2DEG response due to the interactions of the ground-state electrons with X_n. In the case of the Fermi edge singularity, this was accomplished by considering a time-dependent coupled cluster expansion expression for $|\psi_{1L}\rangle$, which describes an exciton dressed by an infinite number of e-h pairs.[14] In the QHS, previous Fermi's golden rule calculations of quasiexciton[31] and trion[43] contributions to the photoluminescence at fractional ν used a basis of 1-h+(N_e+1)-e Slater determinants to diagonalize H for small N_e. We note that small system exact diagonalizations have been successful in describing both ground state and excitation properties of the QHS.[20,31,43]

Given a set of orthonormal states $|X_i\rangle$ and $|Y_\alpha\rangle$, where $\langle Y_\alpha|\hat{X}^\dagger|G\rangle=0$, that describe the main 1-h+(N_e+1)-e configurations of interest, we can express any density matrix $\langle\hat{Z}\rangle^L$ in terms of the linearized density matrices

$$P_i^L = \frac{\langle|G\rangle\langle X_i|\rangle^L}{\sqrt{N}}, \quad \bar{P}_\alpha^L = \frac{\langle|G\rangle\langle Y_\alpha|\rangle^L}{\sqrt{N}}. \quad (25)$$

For example, for $N_e=1$, the X_i states can be chosen as an e-h pair plus a second electron in its ground-state configuration (i.e., the states $|X_n\rangle$) while the Y_α states describe two electrons in states unoccupied in the ground state plus one hole. Using the relations

$$H|X_i\rangle = \Omega_i|X_i\rangle - \sum_{j\neq i} V_{ji}|X_j\rangle + \frac{1}{\sqrt{N}}\sum_\alpha W_{\alpha i}|Y_\alpha\rangle \quad (26)$$

and

$$H|Y_\alpha\rangle = \bar{\Omega}_\alpha|Y_\alpha\rangle + \frac{1}{\sqrt{N}}\sum_i W_{\alpha i}^*|X_i\rangle + \frac{1}{N}\sum_{\alpha'\neq\alpha} W_{\alpha\alpha'}^*|Y_{\alpha'}\rangle, \quad (27)$$

where

$$\Omega_i = \langle X_i|H|X_i\rangle, \quad \bar{\Omega}_\alpha = \langle Y_\alpha|H|Y_\alpha\rangle,$$

$$V_{ij} = -\langle X_i|H|X_j\rangle, \quad W_{\alpha\alpha'} = N\langle Y_\alpha|H|Y_{\alpha'}\rangle,$$

$$W_{\alpha i} = \sqrt{N}\langle Y_\alpha|H|X_i\rangle, \quad (28)$$

which are exact within the subspace of interest, we obtain the following closed system of equations of motion:

$$i\partial_t P_i^L = (\Omega_i - i\Gamma_i)P_i^L - \sum_{j\neq i} V_{ij}P_j^L - d(t)\langle X_i|\hat{X}^\dagger|G\rangle/\sqrt{N} + \frac{1}{\sqrt{N}}\sum_\alpha W_{i\alpha}\bar{P}_\alpha^L, \quad (29)$$

where we introduced the dephasing rates Γ_i, and

$$i\partial_t \bar{P}_\alpha^L = (\bar{\Omega}_\alpha - i\gamma_\alpha)\bar{P}_\alpha^L + \frac{1}{\sqrt{N}}\sum_i W_{\alpha i}P_n^L + \frac{1}{N}\sum_{\alpha'\neq\alpha} W_{\alpha\alpha'}\bar{P}_{\alpha'}^L, \quad (30)$$

where we introduced the dephasing rates γ_α. By choosing a basis of many-body eigenstates of H, $W_{\alpha i}=V_{ij}=0$ and the above equations of motion decouple. This however requires a precise calculation of all excited many-body eigenstates. Given any convenient set of 1-h+(N_e+1)-e states, Eqs. (29) and (30) can be used to calculate, in the time domain, any interband density matrix [to $O(E)$], including dephasing, without solving the eigenvalue problem. Such a nonperturbative solution, exact within a given subspace, is analogous to the Green's-function calculations of relaxation in the manganites and the Hubbard Hamiltonian[51,52] and applies for any correlated ground state.

V. INTRABAND DENSITY MATRICES

In this section we obtain the $O(E^2)$ contributions to any intraband density matrix $\langle\hat{M}\rangle$, where $\hat{M}$ conserves the number of holes. Without loss of generality we assume that the ground-state contribution has already been subtracted out and $\langle G|\hat{M}|G\rangle=0$. Examples of such density matrices are the carrier populations and intraband coherences between many-body states with the same number of electrons and holes. We first note that the 2-h contribution to $\langle\hat{M}\rangle$ is of $O(E^4)$. Within the 1-h subspace, $\langle\hat{M}\rangle$ can be expressed in terms of the Hubbard operator density matrices $\langle|X_i\rangle\langle X_j|\rangle$, $\langle|X_i\rangle\langle Y_\alpha|\rangle$, and $\langle|Y_\alpha\rangle\langle Y_{\alpha'}|\rangle$ for the chosen 1$-h$+(N_e+1)$-e$ states. Within a wave-function approach, these density matrices can be expressed as products of the interband amplitudes P_i^L and $\bar{P}_\alpha^L$. However, relaxation introduces additional intraband dynamics, described by nonfactorizable contributions to the above density matrices,

$$N_{ij} = \frac{1}{N}\langle|X_i\rangle\langle X_j|\rangle - P_j^L P_i^{L*} \quad (31)$$

describes the coherent $X_i \leftrightarrow X_j$ coupling,

$$M_{j\alpha} = \frac{1}{N}\langle|X_j\rangle\langle Y_\alpha|\rangle - P_j^{L*}\bar{P}_\alpha^L \quad (32)$$

describe coherences between the X_i and Y_α states, and

$$N_{\alpha\alpha'} = \frac{1}{N}\langle|Y_\alpha\rangle\langle Y_{\alpha'}|\rangle - \bar{P}_\alpha^{L*}\bar{P}_{\alpha'}^L \quad (33)$$

describe the coupling of the Y_α states. A nonperturbative scheme for describing the full intraband dynamics within the subspace of interest is obtained similar to the previous sec-

tion by noting that Eqs. (26) and (27) allow for a closed system of equations of motion for the above Hubbard operator density matrices. From Eq. (B1) we obtain to $O(E^2)$

$$i\partial_t N_{ij} = (\Omega_j - \Omega_i - i\Gamma_{ij})N_{ij} + i(\Gamma_i + \Gamma_j - \Gamma_{ij})P_j^L P_i^{L*} + \sum_{i' \neq i} V_{i'i}N_{i'j} - \sum_{j' \neq j} V_{jj'}N_{ij'} + \frac{1}{\sqrt{N}}\sum_{\alpha}(W_{\alpha j}^* M_{i\alpha} - W_{\alpha i}M_{j\alpha}^*), \tag{34}$$

$$i\partial_t M_{i\alpha} = (\bar{\Omega}_\alpha - \Omega_i - i\Gamma_{i\alpha})M_{i\alpha} + i(\Gamma_i + \gamma_\alpha - \Gamma_{i\alpha})P_n^{L*}\bar{P}_\alpha^L + \frac{1}{\sqrt{N}}\sum_{i'} W_{\alpha i'}N_{ii'} - \frac{1}{\sqrt{N}}\sum_{\alpha'} W_{\alpha' i}N_{\alpha'\alpha} + \sum_{i' \neq n} V_{i'i}M_{i'\alpha} + \frac{1}{N}\sum_{\alpha' \neq \alpha} W_{\alpha\alpha'}M_{i\alpha'}, \tag{35}$$

and

$$i\partial_t N_{\alpha\alpha'} = (\bar{\Omega}_{\alpha'} - \bar{\Omega}_\alpha - i\Gamma_{\alpha\alpha'})N_{\alpha\alpha'} + i(\gamma_\alpha + \gamma_{\alpha'} - \Gamma_{\alpha\alpha'})\bar{P}_\alpha^{L*}\bar{P}_{\alpha'}^L + \frac{1}{\sqrt{N}}\sum_i (W_{\alpha' i}M_{i\alpha}^* - W_{\alpha i}^* M_{i\alpha'}) + \frac{1}{N}\sum_{\alpha'' \neq \alpha'} W_{\alpha''\alpha'}^* N_{\alpha\alpha''} - \frac{1}{N}\sum_{\alpha'' \neq \alpha} W_{\alpha''\alpha}N_{\alpha'\alpha''}^*. \tag{36}$$

The interaction matrix elements and excitation energies entering in the above equations are the same as in the linear absorption calculation. We note that the above nonfactorizable density matrices vanish in the coherent limit, defined as $\Gamma_{ij}=\Gamma_i+\Gamma_j$, $\Gamma_{i\alpha}=\Gamma_i+\gamma_\alpha$, and $\Gamma_{\alpha\alpha'}=\gamma_\alpha+\gamma_{\alpha'}$. However, as already known from the undoped system,[50] the deviations from this limit are strong and result, e.g., in long-lived incoherent carrier populations and intraband coherence. The closed system [Eqs. (34)–(36)] can be used to describe the light-induced population and intraband coherence dynamics for any ν.

VI. THIRD-ORDER NONLINEAR POLARIZATION

In this section we obtain, to $O(E^3)$, an expression for the interband density matrix $\langle\hat{Z}\rangle$, where $\hat{Z}$ is any operator that reduces the number of holes by one. Our result separates the contributions that can be expressed as products of the linear polarizations P_n^L, whose dependence on the dynamical 2DEG response, was described in Sec. IV, from fully correlated contributions with different dynamics. Our main goal is to use this expression to calculate the $O(E^3)$ contribution to the interaction-induced density matrix $\langle\hat{Y}_n\rangle$ in the nonlinear polarization equation of motion, Eq. (14). We separate out the contribution from the states $\hat{Y}_n^\dagger|G\rangle$, which describe X_n-2DEG interactions that can be treated by using equations of motion and expansions similar to Sec. IV, from the contributions due to interactions of X_n with photoexcited carriers.

Similar to the DCTS,[8,53] we first expand in terms of the optical field and note the one to one correspondence between the photon absorption/emission and the e-h pair creation/destruction processes. The nonlinear response arises from multiple e-h pair creation/destruction processes. During each transition, the photoexcited e-h pair interacts with the 2DEG, as described by P_n^L. In the nonlinear optical response, we must also consider the correlations among the different photoexcited e-h pairs, such as, e.g., four-particle correlations between two photoexcited e's and two photoexcited h's.[1,11,60] In the undoped system, the DCTS cumulant expansions separate the contributions to the density matrices due to correlated and uncorrelated e-h pair transitions.[2,8,9] Here we accomplish this for a strongly correlated populated ground state, where Wick's theorem does not apply as in the DCTS. For this we introduce a decomposition of the many-body state $|\psi(t)\rangle$, which evolves from the exact ground state $|G\rangle$ according to $H(t)$, into correlated and uncorrelated parts. In this way we separate out the parts of $|\psi(t)\rangle$ whose amplitudes can be expressed in terms of products of the linear coherent amplitudes. Such factorizable contributions assume that, although the photoexcited excitons or quasiexcitons are strongly correlated with the 2DEG, their interactions with each other can be treated within a mean-field approximation. Our scheme recovers the DCTS in the undoped system.

Since here electrons are present prior to the photoexcitation, when following the effects of the applied fields we count the number of valence-band holes in a given state. Therefore, we use the shorthand notation 0-h, 1-h, 2-h, …, to label the many-body states. We then express the many-body state as $|\psi\rangle=|\psi_0\rangle+|\psi_1\rangle+|\psi_2\rangle$, where $|\psi_n\rangle$ is the projection to the n-h subspace.[15,17] It is clear that states with three or more holes do not contribute to the third-order nonlinear polarization when the Hamiltonian H conserves the number of holes,

$$\langle\hat{Z}\rangle = \langle\psi_0|\hat{Z}|\psi_1\rangle + \langle\psi_{1L}|\hat{Z}|\psi_2\rangle + O(E^5). \tag{37}$$

Next we consider the linearized time-evolved state $|\psi_{1L}\rangle$, calculated in the previous section, and separate the linear polarization contribution by projecting the $|X_n\rangle$ states,

$$|\psi_{1L}\rangle = \sum_n \frac{\langle\hat{X}_n\rangle^L}{1-\nu_n}|X_n\rangle + |\bar{\psi}_{1L}\rangle, \tag{38}$$

where $\langle X_n|\bar{\psi}_{1L}\rangle=0$. $|\bar{\psi}_{1L}\rangle$ satisfies the equation of motion [Eq. (E6)] and describes X+2DEG* configurations, including trion configurations, which contribute to the optical spectra via their coupling to the X configurations in the many-body 1-h eigenstates of H. The two-photon processes excite two e-h pairs on top of the 2DEG, whose time evolution is given by

$$i\partial_t|\psi_2\rangle = H|\psi_2\rangle - d(t)\hat{X}^\dagger|\psi_{1L}\rangle + O(E^4). \tag{39}$$

Similar to the time evolution of $|\psi_{1L}\rangle$ discussed in the previous section, $|\psi_2\rangle$ can be obtained by introducing a basis of 2-h+(N_e+2)-e states.[60,62] Given the complexity of treating such states, we decompose $|\psi_2\rangle$ into an uncorrelated part, which assumes that each photoexcited e-h pair evolves independently by interacting with the 2DEG, and a correlated part, which describes correlations among the photoexcited e-h pairs,

$$|\psi_2\rangle = \frac{1}{2}\sum_{nm} \frac{\langle \hat{X}_n\rangle^L \langle \hat{X}_m\rangle^L}{(1-\nu_n)(1-\nu_m)} \hat{X}_n^\dagger \hat{X}_m^\dagger |G\rangle + \sum_n \frac{\langle \hat{X}_n\rangle^L}{1-\nu_n} \hat{X}_n^\dagger |\bar{\psi}_{1L}\rangle + |\bar{\psi}_2\rangle + O(E^4). \quad (40)$$

The first term on the rhs of the above equation comes from two independent optical transitions X_n and X_m, which create two e-h pairs that interact independently with the 2DEG but not with each other. The second term describes $\{1\text{-}h/2\text{DEG}^*\}$ configurations, which contribute to the optical response via their coupling to X_m in the many-body eigenstates, that interact with the 2DEG independently of X_n. For example, for $N_e=1$, the first term on the rhs of Eq. (40) describes two zero-momentum e-h pairs plus an electron in its ground-state configuration. During the time evolution, each pair interacts separately with the 2DEG and thus the amplitude of this configuration in the 2-h many-body wave function is the product of the linear polarizations, as in $|\psi_{1L}\rangle$ Eq. (38). The second term describes two electrons in excited configurations correlated with a hole plus a second e-h pair with zero momentum. This term describes the time evolution of a noninteracting trion and exciton configuration. $|\bar{\psi}_2\rangle$ then describes a biexciton state interacting with the 2DEG or a correlated five-particle complex.

$$i\partial_t|\bar{\psi}_2\rangle - H|\bar{\psi}_2\rangle = \frac{1}{2}\sum_{nm}\langle \hat{X}_n\rangle^L\langle \hat{X}_m\rangle^L[\hat{Y}_n^\dagger,\hat{X}_m^\dagger]|G\rangle + \sum_n [\langle \hat{X}_n\rangle^L \hat{Y}_n^\dagger - \langle \hat{Y}_n\rangle^L \hat{X}_n^\dagger]|\bar{\psi}_{1L}\rangle. \quad (41)$$

The first term on the rhs of the above equation describes the time evolution of the correlated four-particle excitation $[\hat{Y}_\alpha^\dagger,\hat{X}_m^\dagger]|G\rangle$ analogous to the undoped system.[1,11] For the ideal 2D system Hamiltonian H,

$$[\hat{X}_m,\hat{Y}_n] = \frac{1}{2\pi\ell^2 N}\sum_{\mathbf{q}m'm''} v_q \times [\phi_{nm'}(-\mathbf{q})\hat{X}_{\mathbf{q}m'n} - \phi_{m'n}(-\mathbf{q})\hat{X}_{\mathbf{q}nm'}] \times [\phi_{mm''}(\mathbf{q})\hat{X}_{-\mathbf{q}m''m} - \phi_{m''m}(\mathbf{q})\hat{X}_{-\mathbf{q}mm''}]. \quad (42)$$

This contribution vanishes if we project to a single LL in the ideal 2D system, due to the hidden symmetry.[56] It also describes biexciton effects as in the undoped system.[1,11,60] The last term in Eq. (41) describes correlations between X and $\{1\text{-}h/2\text{DEG}^*\}$ configurations or two $\{1\text{-}h/2\text{DEG}^*\}$ configurations. In an analogous way, we decompose the $O(E^2)$ contribution to the 0-h state $|\psi_0\rangle$, created by two-photon Raman processes of excitation and then de-excitation of an e-h pair, as

$$|\psi_0\rangle = \langle G|\psi\rangle|G\rangle - \sum_n \frac{\langle \hat{X}_n\rangle^{L*}}{1-\nu_n}\hat{X}_n|\bar{\psi}_{1L}\rangle + |\bar{\psi}_0\rangle + O(E^4). \quad (43)$$

where $\langle G|\bar{\psi}_0\rangle=0$. The $\{0\text{-}h/2\text{DEG}^*\}$ state $|\bar{\psi}_0\rangle$ is determined by the equation of motion, Eq. (E5). Equations (41) and (E5) can be solved similar to the undoped system[60] by projecting to a subspace of 2-h and 0-h states.

By substituting the wave-function decompositions, Eqs. (38), (40), and (43), to Eq. (37) we obtain the following exact expression for $\langle \hat{Z}\rangle$, which separates out all nonlinear contributions that are proportional to the linear polarizations P_n^L.[15,17]

$$\langle \hat{Z}\rangle = \sum_n \frac{\langle \hat{X}_n\rangle^{L*}}{1-\nu_n}\langle G|[\hat{X}_n,\hat{Z}]|\psi_2\rangle + \frac{1}{2}\sum_{nn'}\frac{\langle \hat{X}_n\rangle^L\langle \hat{X}_{n'}\rangle^L}{(1-\nu_n)(1-\nu_{n'})}\langle \bar{\psi}_{1L}|[[\hat{Z},\hat{X}_n^\dagger],\hat{X}_n^\dagger]|G\rangle + \sum_n \frac{\langle \hat{X}_n\rangle^L}{1-\nu_n}\langle [\hat{Z},\hat{X}_n^\dagger]\rangle_c + \langle |G\rangle\langle G|\hat{Z}\rangle + \sum_n \frac{\langle \hat{X}_n\rangle^{L*}}{1-\nu_n}\langle G|\hat{Z}\hat{X}_n|\psi_2\rangle - \frac{\langle \hat{X}_n\rangle^L}{1-\nu_n}\langle G|\hat{Z}X_n^\dagger|\bar{\psi}_0\rangle + \langle \bar{\psi}_{1L}|\hat{Z}|\bar{\psi}_2\rangle + \langle \bar{\psi}_0|\hat{Z}|\bar{\psi}_{1L}\rangle. \quad (44)$$

By using Eq. (44) to obtain the interaction-induced density matrix $\langle \hat{Y}_n\rangle$ in Eq. (14), we establish the connection to the known results for the ultrafast nonlinear optical response of undoped semiconductors.[2,9] The first term on the rhs of Eq. (44) describes the X-X interband coherence and recovers the well-known treatment of X-X interactions in undoped semiconductors.[53,60] The 2-h state amplitude $\langle G|[\hat{X}_m,\hat{Y}_n]|\psi_2\rangle$ coincides to $O(E^2)$ with the density matrices $\langle [\hat{X}_m,\hat{Y}_n]\rangle$ and $\langle |G\rangle\langle G|[\hat{X}_m,\hat{Y}_n]\rangle$, which in turn can be expressed in terms of X-X density matrices $\langle \hat{X}\hat{X}\rangle$ [see Eq. (42)]. The dynamics and dephasing of this X-X coherence can be described by using Eqs. (40) and (41). The familiar decomposition of the X-X coherence into Hartree-Fock and correlated parts[11,53,60] is obtained by using Eq. (40) for $|\psi_2\rangle$. Similar to the undoped system,[53] Eq. (41) can be used to express the effects of the X-X correlations in terms of a memory kernel determined by the dynamics within the 2-h subspace.

The second and third terms on the rhs of Eq. (44) come from the interaction of the interband polarization with intraband coherences and populations and describe light-induced time-dependent corrections to the X energies and inter-LL couplings. The third term is determined by the nonfactorizable intraband density matrix

$$\langle [\hat{Z},\hat{X}_n^\dagger]\rangle_c = \langle [\hat{Z},\hat{X}_n^\dagger]\rangle - \sum_{n'm'}\frac{\langle \hat{X}_n'\rangle^{L*}\langle \hat{X}_{m'}\rangle^L}{(1-\nu_{n'})(1-\nu_{m'})}\langle X_{n'}|[\hat{Z},\hat{X}_n^\dagger]|X_{m'}\rangle - \sum_{n'}\frac{\langle \hat{X}_{n'}\rangle^{L*}}{1-\nu_{n'}}\langle G|[\hat{X}_{n'},[\hat{Z},\hat{X}_n^\dagger]]|\bar{\psi}_{1L}\rangle - \sum_{n'}\frac{\langle \hat{X}_{n'}\rangle^L}{1-\nu_{n'}}\langle \bar{\psi}_{1L}|[[\hat{Z},\hat{X}_n^\dagger],\hat{X}_{n'}^\dagger]|G\rangle, \quad (45)$$

which in terms of many-body states is given by

$$\langle[\hat{Z},\hat{X}_n^\dagger]\rangle_c = \langle\bar{\psi}_{1L}|[\hat{Z},\hat{X}_n^\dagger]|\bar{\psi}_{1L}\rangle + \langle G|[\hat{Z},\hat{X}_n^\dagger]|\bar{\psi}_0\rangle + \langle\bar{\psi}_0|[\hat{Z},\hat{X}_n^\dagger]|G\rangle. \tag{46}$$

In the undoped system, this term describes X scattering from incoherent X populations and $X\leftrightarrow X$ coherences due to X-X interactions and relaxation.[2]

The fourth, fifth, and sixth terms on the rhs of Eq. (44) describe a contribution determined by the state $\hat{Z}^\dagger|G\rangle$. Since here $\hat{Z}^\dagger$ acts on the ground state, as in the calculation of the linearized density matrix in Sec. IV, this contribution for $\hat{Z}=\hat{Y}_n$ describes an X-2DEG coupling similar to Eq. (11) and the calculation of the linear polarization. This contribution describes the trion formation and can be described by its equation of motion after expanding $\hat{Z}^\dagger|G\rangle$ in terms of the basis states $|X_i\rangle$ and $|Y_\alpha\rangle$. We can thus obtain a closed system of equations of motion similar to Sec. IV. The last two terms in Eq. (44) can also be obtained from the equations of motion [Eqs. (41) and (E6)] after projecting the 1-h and 0-h basis states. Noting that here $\hat{Z}^\dagger$ acts on $\{1\text{-}h/2\text{DEG}^*\}$ configurations and not the ground state, $\langle\bar{\psi}_{1L}|\hat{Y}_n|\bar{\psi}_2\rangle$ describes both trion-trion and exciton-trion interactions. In the undoped system, it describes the incoherent exciton-biexciton transition contribution determined by the fully correlated part of the density matrices $\langle X^\dagger XX\rangle$.[9] In the next section we use the above results to study the role of the LL0$\rightarrow$LL1 excitations of an incompressible quantum liquid in the ideal 2D system.

VII. NUMERICAL RESULTS

In this section we describe the optical dynamics of the ideal 2D system at $\nu=1$. This ground state simplifies the calculation of the interaction matrix elements and excitation energies and allows us to highlight in a simple way the qualitative dynamical features that can arise from X interactions with an incompressible quantum liquid. For this we develop a model that describes the dynamical inter-LL coupling revealed by the FWM experiments of Chemla and co-workers.[45–47]

A. Description of the model

At $\nu=1$, the 2DEG in the ground-state Laughlin wave function[21] populates all N of the spin-$\uparrow$ LL0 states while all spin-$\downarrow$ LL0 states and all higher LLs are empty. Signatures of spin polarization were observed in linear absorption experiments[22,61] at temperatures as high as a few kelvin.[63]

$$\hat{\rho}^e_{\mathbf{q}00\uparrow}|G\rangle = \delta_{q,0}\sqrt{N}|G\rangle \tag{47}$$

for the $\nu=1$ ground state in which case the lowest 2DEG neutral excitations are LL0$\rightarrow$LL1 excitations. Also, the screening of the interaction is suppressed due to the LL0-LL1 energy gap.[25] Equation (16) then reduces to

$$\hat{Y}_1 = -\hat{Y}_0 = \hat{Y}, \tag{48}$$

where

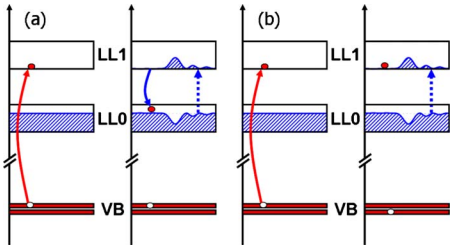

FIG. 1. (Color online) Interaction-induced coupling of X_1 and (a) the $\{1\text{-LL0-}e+1\text{-LL1-}h+\text{LL0}\rightarrow\text{LL1}\}$ four-particle excitations $|Y_\mathbf{q}\rangle$ (resonant process) and (b) $\{1\text{-LL1-}e+1\text{-LL0-}h+\text{LL0}\rightarrow\text{LL1}\}$ excitations (nonresonant process).

$$\hat{Y} = \frac{1}{2\pi\ell^2\sqrt{N}}\sum_{\mathbf{q}\neq 0} v_q\hat{\rho}_\mathbf{q}[\phi_{10}(-\mathbf{q})\hat{X}_{\mathbf{q}01} - \phi_{01}(-\mathbf{q})\hat{X}_{\mathbf{q}10}]. \tag{49}$$

Due to the hidden symmetry,[56] $\hat{Y}$ vanishes if we project within a single LL. We thus retain both LL0 and LL1 carrier states. For optical pulses tuned to excite LL0 and LL1 transitions, we neglect states with energy comparable to LL2 or higher, whose contribution is suppressed due to their small energetic overlap with the optical pulses in the FWM experiments. The FWM experiments in the QHS (Refs. 45–47) did not show any significant FWM signal at LL2 or higher energies. However, their results indicate a strong dynamical coupling of the LL0 and LL1 resonances, which differ by an energy $\sim$18 meV on the order of the electron cyclotron energy. We thus break the hidden symmetry by considering the LL0-LL1 mixing due to inter-LL 2DEG excitations. Since states with two or more inter-LL excitations have energy comparable to LL2 or higher, we solve a polaronic problem where the magnetoexciton states $|X_0\rangle$ and $|X_1\rangle$ couple to a continuum of $X_0+(\text{LL0}\rightarrow\text{LL1})$ MP or MR configurations. Neglecting configurations with energy comparable to LL2 or higher in the many-body eigenstates is justified for sufficiently large magnetic fields, when the Coulomb-to-cyclotron energy ratio $e^2/(\epsilon l\omega_c^e)$ becomes smaller than 1. We note however that, in GaAs, the Coulomb-to-cyclotron energy ratio is comparable to 1 for the magnetic fields up to $\sim$10 T in FWM experiments For example, at 10 T, $\omega_c\sim 18$ meV for electrons while the characteristic Coulomb energy is $e^2/\epsilon l\sim 14$ meV. Therefore, quantitative comparisons with experiments must include higher LLs. Nevertheless, we expect that the higher energy states will not change the qualitative features, as is often the case for the 2DEG excitation spectrum.[27,28]

In the case of X_1 in the QHS, the e-2DEG interaction scatters the LL1 electron to LL0 by emitting a LL0$\rightarrow$LL1 2DEG excitation at small total energy cost [see Fig. 1(a)]. This resonant interaction process couples X_1 to the $\{1\text{-}h/2\text{DEG}^*\}$ orthonormal states

$$|Y_\mathbf{q}\rangle = \hat{Y}^\dagger_\mathbf{q}|G\rangle = \hat{X}^\dagger_{\mathbf{q}01}\hat{\rho}^e_{-\mathbf{q}10\uparrow}|G\rangle \tag{50}$$

that enter in Eq. (49). We include this *continuum* of basis states to our subspace, which allows us to treat the quantum kinetics of the $X_1\rightarrow X_{01}+\text{MP}$ scattering process nonperturba-

tively in the Coulomb interaction, rather than use the semiclassical Fermi's golden rule. Due to the resonance between the X_1 and $Y_{\mathbf{q}}$ states, their coupling is strong. In the ideal 2D system, $|Y_0\rangle$, Eq. (11), is a linear combination of the same states as $|Y_1\rangle$ due to the hidden symmetry [Eq. (48)]. However, their energies are higher than that of $|X_0\rangle$. Therefore, the X_0-2DEG interactions, treated here on the same basis as the X_1-2DEG scattering, are suppressed in the ideal 2D system for sufficiently large magnetic fields. We show below that this asymmetry between the two QHS magnetoexcitons is important for understanding the optical dynamics.

Turning to the h-2DEG scattering, we note that the X_1 hole can scatter to LL0 by emitting a LL0$\rightarrow$LLn 2DEG excitation, which leads to the $\{1\text{-LL1-}e+1\text{-LL0-}h+\text{LL0}\rightarrow\text{LL}n\}$ final states in Eq. (49) [see Fig. 1(b)]. However, noting that the hole cyclotron energy is ~ 4 meV at 10 T, the energy of these states is close to that of LL2 or higher and therefore their contribution to the optical response at the LL1 and LL0 energies is suppressed. The only other $\{1\text{-}h/2\text{DEG}^*\}$ excitations with energies comparable to LL0 or LL1 are the $\{1\text{-LL0-}e+1\text{-LL}n\text{-}h+\text{LL0}\rightarrow\text{LL1}\}$ configurations, where $n=0,2,\ldots$, which in the ideal 2D system couple to $Y_{\mathbf{q}}$ via inter-LL hole scattering, However, such configurations are not expected to change significantly the LL0-LL1 resonance coupling observed in the experiments and we neglect them for simplicity, after noting that the complicated valence band structure must be treated for quantitative comparisons to experiment and that the characteristic disorder energy is often comparable to the hole cyclotron energy. Below we calculate the full optical dynamics within the subspace spanned by $|X_n\rangle$, $n=0,1$, and the continuum of $|Y_{\mathbf{q}}\rangle$ states, Eq. (50).

B. Linear absorption at $\nu=1$

In this section we present our results for the linear absorption spectrum. From Eq. (28) we obtain by using Eqs. (48)–(50) that the X_n-$Y_{\mathbf{q}}$ interaction,

$$W_{\mathbf{q}n}=W_{n\mathbf{q}}=(\delta_{n,1}-\delta_{n,0})v_{01}^{01}(\mathbf{q}), \tag{51}$$

is proportional to the interaction potential

$$v_{nn'}^{mm'}(q)=\frac{1}{2\pi l^2}v_q\phi_{mm'}^*(\mathbf{q})\phi_{nn'}(\mathbf{q}). \tag{52}$$

Equations (29) and (30) then reduce to

$$i\partial_t P_0^L=(\Omega_0-i\Gamma_0)P_0^L-V_{01}P_1^L-d(t)-\frac{1}{\sqrt{N}}\sum_{\mathbf{q}}v_{01}^{01}(\mathbf{q})\bar{P}_{\mathbf{q}}^L \tag{53}$$

for the LL0 polarization and to

$$i\partial_t P_1^L=(\Omega_1-i\Gamma_1)P_1^L-V_{10}P_0^L-d(t)+\frac{1}{\sqrt{N}}\sum_{\mathbf{q}}v_{01}^{01}(\mathbf{q})\bar{P}_{\mathbf{q}}^L \tag{54}$$

for the LL1 polarization. The exciton dephasing rates, $\Gamma_0=\Gamma_1=0.5$ meV, are chosen similar to the undoped system. The energies of the X states are given by

$$\Omega_n=E_g+\left(n+\frac{1}{2}\right)(\omega_c^e+\omega_c^h)-V_{nn}, \tag{55}$$

where, as obtained from Eq. (28),

$$V_{nm}=\int\frac{d\mathbf{q}}{(2\pi)^2}v_q|\phi_{nm}(\mathbf{q})|^2 \tag{56}$$

are the X binding energies ($n=m$) and static inter-LL coupling energies ($n\neq m$). The equations of motion for the $Y_{\mathbf{q}}$ coherences are obtained from Eqs. (30) and (51),

$$i\partial_t\bar{P}_{\mathbf{q}}^L=(\bar{\Omega}_{\mathbf{q}}-i\gamma)\bar{P}_{\mathbf{q}}^L+\frac{v_{01}^{01}(\mathbf{q})}{\sqrt{N}}(P_1^L-P_0^L)+\frac{1}{N}\sum_{\mathbf{q}'\neq\mathbf{q}}W_{\mathbf{q}\mathbf{q}'}\bar{P}_{\mathbf{q}'}^L, \tag{57}$$

where we introduced a Y-excitation dephasing rate $\gamma=0.35$ meV. The coupling between P_n^L and $\bar{P}_{\mathbf{q}}^L$ in the above equations of motion gives eigenstates that are a linear combination of X and $Y_{\mathbf{q}}$ configurations. From Eq. (28), we obtain after using Eqs. (C1) and (B5),

$$W_{\mathbf{q}\mathbf{q}'}=W_{\mathbf{q}'\mathbf{q}}=2v_{11}^{00}(\mathbf{q}'-\mathbf{q})\cos[(\mathbf{q}\times\mathbf{q}')_z\ell^2]-v_{11}^{11}(\mathbf{q}'-\mathbf{q})-v_{00}^{00}(\mathbf{q}'-\mathbf{q}). \tag{58}$$

The interaction $W_{\mathbf{q}\mathbf{q}'}$ leads to rescattering among the continuum of $Y_{\mathbf{q}}$ states with different momenta, which corresponds to nonperturbative vertex corrections beyond the Born approximation. The Y-state dispersion $\bar{\Omega}_{\mathbf{q}}=\Omega_{\mathbf{q}01}+\omega_{-\mathbf{q}}$ is obtained in Appendix C. $\Omega_{\mathbf{q}01}$, Eq. (C4), is the X_{01} excitation energy and $\omega_{\mathbf{q}}$, Eq. (C5), is the energy of the LL0$\rightarrow$LL1 2DEG excitations, given by[25]

$$\omega_{\mathbf{q}}-\omega_c^e=\frac{e^2}{\epsilon\ell}\frac{q\ell}{2}e^{-q^2\ell^2/2}+\frac{e^2}{\epsilon\ell}\frac{1}{2}\sqrt{\frac{\pi}{2}}\left\{1-e^{-q^2\ell^2/4}\left[\left(1+\frac{q^2\ell^2}{2}\right)I_0\left(\frac{q^2\ell^2}{4}\right)-\frac{q^2\ell^2}{2}I_1\left(\frac{q^2\ell^2}{4}\right)\right]\right\}, \tag{59}$$

where I_n is a modified Bessel function of the first kind and ϵ is the dielectric constant. The first term on the rhs of the above equation corresponds to the RPA treatment of the 2DEG interactions. The second term results from the many-body corrections to the local field seen by an electron, which at $\nu=1$ correspond to exchange effects. These local-field cor-

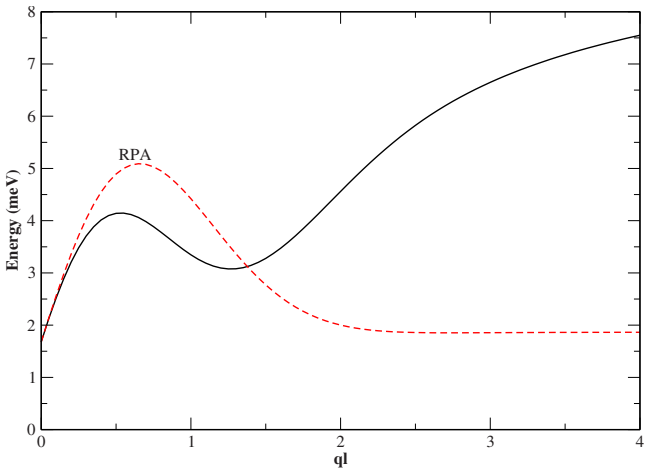

FIG. 2. (Color online) Energy dispersion $\bar{\Omega}_{\mathbf{q}}$ of the $Y_{\mathbf{q}}$ states, measured with respect to the X_1 energy at $\nu=1$. Solid line: correlated 2DEG. Dotted line: RPA approximation. $B=8.7$ T as in the experiment.

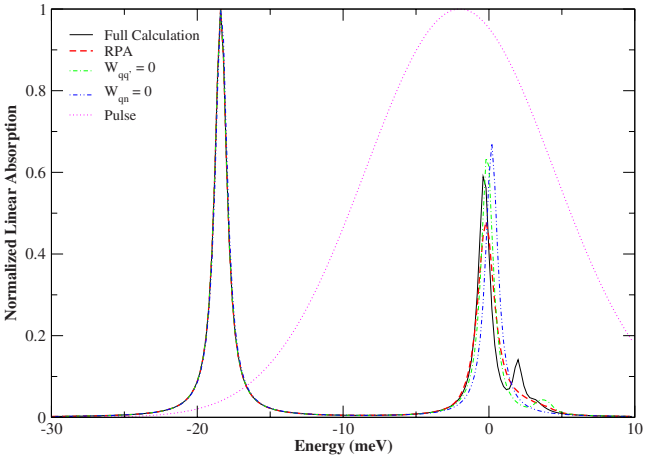

FIG. 3. (Color online) Linear absorption spectrum. Solid line: full calculation. Dashed-double dotted line: $W_{\mathbf{q}n}=0$. Dashed line: absorption using the RPA dispersion. Dashed-dotted line: $W_{\mathbf{q}\mathbf{q}'}=0$. Also shown is the overlap of the optical pulse with the LL0 and LL1 absorption peaks (dotted line).

rections result in a magnetoroton dispersion minimum absent within the RPA, whose detailed momentum dependence is determined by the ground-state static structure factor at the corresponding filling factor.[27] Analogous dispersions can be obtained for fractional ν by considering a basis set of 2DEG excitations as in Ref. 27.

Figure 2 shows $\bar{\Omega}_{\mathbf{q}}$ at $\nu=1$. The energy dispersion of the $Y_{\mathbf{q}}$ continuum basis of states mainly reflects the momentum dependence of the inter-LL excitation energy $\omega_{\mathbf{q}}$ but also depends on the X_{01} dispersion. The origin of the collective excitation dispersion may be seen by first noting that the lowest energy neutral excitations of a noninteracting 2DEG are the N^2 degenerate LL0$\rightarrow$LL1 incoherent pair excitations, which all have energy ω_c^e. This degeneracy is lifted by the electron-electron interaction, which in the case of an incompressible ground state leads to an energy dispersion of the form shown in Fig. 2. For $q\ell \ll 1$, the momentum dependence of $\bar{\Omega}_{\mathbf{q}}$ is approximately linear, as in the RPA treatment of the 2DEG interactions. However, the RPA fails completely for $q\ell > 1$, where the 2DEG correlations result in a MR dispersion minimum.[20,22,25,27] The drastic change in the $Y_{\mathbf{q}}$ dispersion as compared to the RPA, due to an incompressible ground state, has a significant effect on the X_1-$Y_{\mathbf{q}}$ coupling since it changes the relative energies (see Fig. 2). One of our goals here is to study the effects of the inter-LL MR dispersion minimum on the linear and nonlinear optical properties.

Figure 3 shows the linear absorption spectrum. By comparing to the result obtained with $W_{\mathbf{q}n}=0$, which neglects the polaronic effects due to MP coupling, it is clear that the X_1-$Y_{\mathbf{q}}$ coupling gives a third absorption peak above the LL1 exciton peak and not simple broadening. Importantly, this third peak is suppressed if the $Y_{\mathbf{q}}$ energy dispersion is approximated by using the RPA. In the latter case, the coupling of X_1 to the $Y_{\mathbf{q}}$ continuum broadens the LL1 resonance, which suppresses its strength as compared to the full calculation. The differences between the RPA and full dispersion calculations come from the MR minimum, which enhances the X_1-X_{01}+MR coupling. Figure 3 also shows the results obtained by treating the X-Y coupling perturbatively (Born approximation), obtained by setting $W_{\mathbf{q}\mathbf{q}'}=0$ in Eq. (57). The vertex corrections describe rescattering among the continuum of $Y_{\mathbf{q}}$ states and strongly enhance the third absorption peak.

We conclude from Fig. 3 that the full dynamics of the X+MR excitations and their coupling to X_1 play a crucial role in determining the linear absorption line shape. We obtain a new resonance close to the LL1 energy, resulting from the coupling of X_1 to $\{1\text{MR}+1\text{-LL0-}e+1\text{-LL1-}h\}$ states in the many-body eigenstates, which is suppressed within the RPA treatment of the 2DEG interactions. An analogy could be drawn between the above resonance at $\nu=1$ and the trion resonances at $\nu<1$ (Refs. 40–42 and 55) (for a review, see Ref. 39). Both come from the coupling of X and Y_n configurations in Eq. (14). We note however that X-intra-LL scattering effects are suppressed when the dephasing and disorder characteristic energies are sufficiently strong. For example, in the samples used in the experiments of Refs. 18 and 47, the LL0 resonance displayed a Lorentzian line shape while the FWM signal in the case of photoexcitation at the LL0 energy did not produce any unexpected results. On the other hand, these experiments show the emergence, for $\nu<2$, of an asymmetric LL1 resonance with a strong high-energy shoulder. In the realistic doped quantum well system, the finite confinement, valence-band mixing, and disorder effects change the exciton energies and X_1-$Y_{\mathbf{q}}$ coupling as compared to our Hamiltonian, which affects the relative magnitudes and energies of the two LL1 peaks. Our calculation gives a linear absorption line shape similar to the experiment if we consider X_1-$Y_{\mathbf{q}}$ energy splittings smaller than in the ideal 2D system and larger dephasing rates. In this case however, the differences between the RPA and full calculations are suppressed.

C. Transient nonlinear optical response

In this section we present our results for the third-order nonlinear polarization. First we use Eq. (42) to express the

X-X coherence $\langle[\hat{X}_m,\hat{Y}_n]\rangle$ in terms of the two-exciton density matrices $\langle\hat{X}\hat{X}\rangle$ and obtain from Eq. (40),

$$\langle\hat{X}_{-\mathbf{q}10}\hat{X}_{\mathbf{q}10}\rangle = \frac{2V_{10}}{N}P_0^L P_1^L + \langle\hat{X}_{-\mathbf{q}10}\hat{X}_{\mathbf{q}10}\rangle_c, \tag{60}$$

where the first term is the Hartree-Fock X-X contribution. On the other hand, $\langle\hat{X}_{-\mathbf{q}mn}\hat{X}_{\mathbf{q}mn}\rangle = \langle\hat{X}_{-\mathbf{q}mn}\hat{X}_{\mathbf{q}mn}\rangle_c$ for $m=0$, $n=1$ and $m=1$, $n=0$. Since the experimental studies of both doped and undoped quantum wells[45,46,50] did not produce any long-lasting FWM signal at negative time delays, which would signify long-lived X-X correlations,[1,11,60] we treat for simplicity the X-X interactions within the Hartree-Fock approximation. The third term on the rhs of Eq. (44) was expressed in Appendix D in terms of the Hubbard operator density matrices N_{nm}, $M_{n\mathbf{q}}$, and $N_{\mathbf{q}\mathbf{q}'}$. We thus obtain from Eqs. (14) and (44) after some algebra

$$i\partial_t P_0 - (\Omega_0 - i\Gamma_0)P_0 + V_{01}P_1 = d(t)n_0 + V_{01}P_1^L(n_0 - 2N_{01}^*) - V_{01}P_0^L(n_1 - 2N_{01}) - P_0^L\sum_{\mathbf{q}} v_{01}^{01}(\mathbf{q})\left[\bar{n}_{\mathbf{q}} + \frac{1}{\sqrt{N}}(M_{1\mathbf{q}}^* - M_{0\mathbf{q}})\right]$$
$$- P_1^L\sum_{\mathbf{q}} v_{01}^{01}(\mathbf{q})\left[\bar{n}_{\mathbf{q}} - \frac{1}{\sqrt{N}}(M_{1\mathbf{q}} - M_{0\mathbf{q}}^*)\right] - \frac{1}{\sqrt{N}}\sum_{\mathbf{q}} v_{01}^{01}(\mathbf{q})P_0^L P_1^L \bar{P}_{\mathbf{q}}^{L*} - \frac{1}{\sqrt{N}}\sum_{\mathbf{q}} v_{01}^{01}(\mathbf{q})\bar{P}_{\mathbf{q}}, \tag{61}$$

$$i\partial_t P_1 - (\Omega_1 - i\Gamma_1)P_1 + V_{01}P_0 = d(t)n_1 - V_{01}P_1^L(n_0 - 2N_{01}^*) + V_{01}P_0^L(n_1 - 2N_{01}) + P_0^L\sum_{\mathbf{q}} v_{01}^{01}(\mathbf{q})\left[\bar{n}_{\mathbf{q}} + \frac{1}{\sqrt{N}}(M_{1\mathbf{q}}^* - M_{0\mathbf{q}})\right]$$
$$+ P_1^L\sum_{\mathbf{q}} v_{01}^{01}(\mathbf{q})\left[\bar{n}_{\mathbf{q}} - \frac{1}{\sqrt{N}}(M_{1\mathbf{q}} - M_{0\mathbf{q}}^*)\right] + \frac{1}{\sqrt{N}}\sum_{\mathbf{q}} v_{01}^{01}(\mathbf{q})P_0^L P_1^L \bar{P}_{\mathbf{q}}^{L*} + \frac{1}{\sqrt{N}}\sum_{\mathbf{q}} v_{01}^{01}(\mathbf{q})\bar{P}_{\mathbf{q}}. \tag{62}$$

The double-peak structure of the linear absorption spectrum close to the LL1 energy implies that the Y and X states couple strongly in the eigenstates of the QHS Hamiltonian, which is described by the coupling between P_n and $\bar{P}_{\mathbf{q}}$. Such linear and nonlinear X-Y couplings are described by the following equation of motion for $\bar{P}_{\mathbf{q}}$, derived in Appendix E:

$$i\partial_t \bar{P}_{\mathbf{q}} - (\bar{\Omega}_{\mathbf{q}} - i\gamma)\bar{P}_{\mathbf{q}} = \frac{v_{01}^{01}(\mathbf{q})}{\sqrt{N}}(P_1 - P_0) + \frac{1}{N}\sum_{\mathbf{q}'} W_{\mathbf{q}\mathbf{q}'}\bar{P}_{\mathbf{q}'} + d(t)(P_1^{L*} + P_0^{L*})\bar{P}_{\mathbf{q}}^L + \frac{v_{01}^{01}(\mathbf{q})}{\sqrt{N}}[P_1^L(N_{11} - P_0^{L*}P_0^L - N_{00}) - P_0^L(N_{00} - P_1^{L*}P_1^L$$
$$- N_{11})] + [v_{01}^{01}(\mathbf{q}) - V_{01}](P_1^L - P_0^L)(P_1^{L*}\bar{P}_{\mathbf{q}}^L + M_{1\mathbf{q}} - P_0^{L*}\bar{P}_{\mathbf{q}}^L - M_{0\mathbf{q}}) + \sum_{\mathbf{q}'}\frac{v_{01}^{01}(\mathbf{q}')}{\sqrt{N}}\bar{P}_{\mathbf{q}'}^L(M_{1\mathbf{q}} - M_{0\mathbf{q}}) + \frac{v_{01}^{01}(\mathbf{q})}{\sqrt{N}}(P_1^L$$
$$- P_0^L)[2N\bar{n}_{\mathbf{q}} - 3\sum_{\mathbf{q}'}\bar{n}_{\mathbf{q}'}] + (P_1^L - P_0^L)\sum_{\mathbf{q}'}\frac{v_{01}^{01}(\mathbf{q}')}{\sqrt{N}}[\bar{P}_{\mathbf{q}'}^{L*}\bar{P}_{\mathbf{q}}^L - 4\bar{n}_{\mathbf{q}'\mathbf{q}}] + \frac{4}{N}(P_1^L$$
$$- P_0^L)\sum_{\mathbf{q}'\mathbf{q}''}\frac{v_{01}^{01}(\mathbf{q}+\mathbf{q}'-\mathbf{q}'')}{\sqrt{N}}\cos^2\left[\frac{l^2}{2}(\mathbf{q}\times\mathbf{q}' + \mathbf{q}'\times\mathbf{q}'' - \mathbf{q}\times\mathbf{q}'')_z\right]\bar{n}_{\mathbf{q}'\mathbf{q}''}. \tag{63}$$

The first two terms on the rhs of Eq. (63) describe linear X-Y couplings, similar to the calculation of the linear polarization, while the rest of the terms describe light-induced nonlinear couplings and polarization dephasing.

The nonlinearities in Eqs. (61)–(63) depend on the LLn carrier populations n_n and on the Y-state populations $\bar{n}_{\mathbf{q}}$. As shown in Appendix D, the total carrier populations, Eq. (15), can be expressed as

$$n_n = 2P_n^L P_n^{L*} + \bar{\nu}_n, \tag{64}$$

where the first term is the coherent X_n population and

$$\bar{\nu}_n = 2N_{nn} + \sum_{\mathbf{q}}\bar{n}_{\mathbf{q}}, \tag{65}$$

obtained by using Eqs. (D16) and (D17), is the incoherent LLn total electron and hole population, with contributions in the QHS from both the X_n and $Y_{\mathbf{q}}$ configurations, N_{nn} and $\bar{n}_{\mathbf{q}}$, respectively. $\bar{n}_{\mathbf{q}} = \bar{n}_{\mathbf{q}\mathbf{q}}$, where

$$\bar{n}_{\mathbf{q}\mathbf{q}'} = \bar{P}_{\mathbf{q}}^{L*}\bar{P}_{\mathbf{q}'}^L + N_{\mathbf{q}\mathbf{q}'}. \tag{66}$$

The coherences $\bar{n}_{\mathbf{q}\mathbf{q}'}$ between Y states with different momenta $\mathbf{q}\neq\mathbf{q}'$ dephase rapidly and are neglected for simplicity. We retain however the $X_n \leftrightarrow Y_{\mathbf{q}}$ coherences $M_{n\mathbf{q}}$, obtained from the equation of motion [Eq. (35)] with dephasing rates

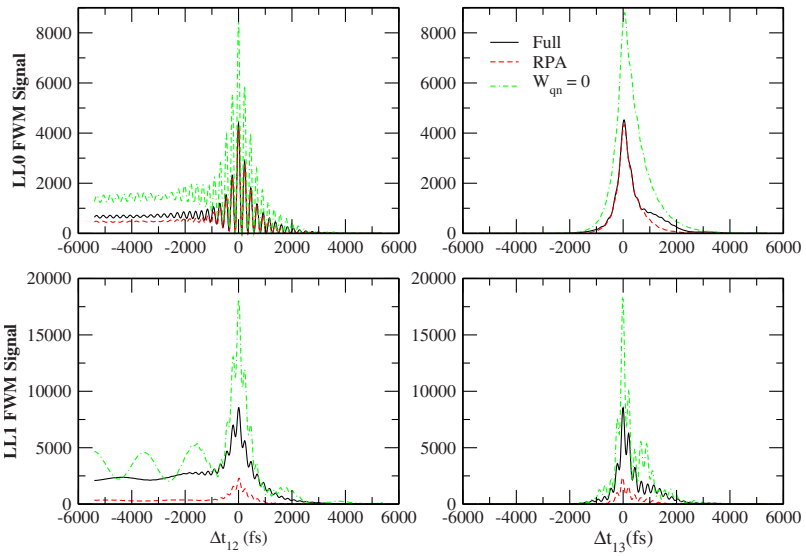

FIG. 4. (Color online) Interaction effects on the FWM signal along the Δt_{12} and Δt_{13} axes for LL1 photoexcitation. Solid line: full calculation. Dashed-dotted line: $W_{\mathbf{q}n}=0$, $V_{01}\neq 0$ (as in the undoped system). Dashed line: RPA $Y_{\mathbf{q}}$ dispersion.

$\gamma_{n\mathbf{q}}=0.5$ meV without resorting to the adiabatic semiclassical approximation.[3] The total populations n_n were obtained from Eqs. (34) and (36) by including the population relaxation rate $\Gamma_{pop}=\Gamma_{\mathbf{qq}}=\Gamma_{nn}=0.001$ meV. Our truncation scheme satisfies the total charge conservation condition,

$$\partial_t(n_0+n_1)=4\ \mathrm{Im}[d^*(t)(P_0^{\mathrm{L}}+P_1^{\mathrm{L}})]-\Gamma_{pop}(n_0+n_1), \quad (67)$$

where the first term on the rhs describes the photoexcited total carrier population. The LL0-LL1 coupling due to the interactions leads to carrier redistribution and coherence between the LLs. Such coupling changes the frequency dependence of the FWM signal as discussed below without however affecting the *total* charge.

D. Three-pulse four-wave mixing: Numerical results

We now consider a three-pulse FWM configuration, where the QHS system is excited by three optical pulses

$$d(t)=\mu E_p(t)e^{i(\mathbf{k}_1\cdot\mathbf{r}-\omega_p t)}+\mu E_p(t+\Delta t_{12})e^{i(\mathbf{k}_2\cdot\mathbf{r}-\omega_p t)}+\mu E_p(t+\Delta t_{13})e^{i(\mathbf{k}_3\cdot\mathbf{r}-\omega_p t)}, \quad (68)$$

where $E_p(t)=E_0e^{-(t/t_p)^2}$ is the pulse amplitude and ω_p its central frequency. The optical fields propagate in the spatially distinct directions $\mathbf{k}_1$, $\mathbf{k}_2$, and $\mathbf{k}_3$, with a time delay Δt_{12} (Δt_{13}) between pulses $\mathbf{k}_1$ and $\mathbf{k}_2$ ($\mathbf{k}_3$). For negative time delays, pulse $\mathbf{k}_1$ arrives first. Importantly, *we tune* ω_p close to LL1 (see Fig. 3), which results in small photoexcitation of LL0 transitions as compared to LL1. This choice suppresses the PSF contribution at the LL0 energy and highlights the interaction effects.

We calculated the third-order FWM signal

$$S(\omega,\Delta t_{12},\Delta t_{13})=|P_0(\omega)+P_1(\omega)|^2 \quad (69)$$

in the background-free direction $\mathbf{k}_1+\mathbf{k}_2-\mathbf{k}_3$, as function of frequency and the two time delays. Here we present the time dependence along the Δt_{12} axis ($\Delta t_{13}=0$) and the Δt_{13} axis ($\Delta t_{12}=0$), calculated in all cases at the two frequencies ω corresponding to the peaks of the LL0 and LL1 FWM resonances. For $\Delta t_{13}>0$, $\Delta t_{12}=0$, pulse $\mathbf{k}_3$ comes first and creates an interband polarization. The latter evolves and decays for a time interval Δt_{13}, when pulses $\mathbf{k}_1$ and $\mathbf{k}_2$ arrive and create the third-order FWM signal. Therefore, the $\Delta t_{13}>0$ axis mainly accesses the decoherence of the interband polarization. Along the negative Δt_{13} axis, pulses $\mathbf{k}_1$ and $\mathbf{k}_2$ first create an *X*-*X* coherence, which evolves and dephases for a time interval $|\Delta t_{13}|$ when pulse $\mathbf{k}_3$ arrives. Therefore, the $\Delta t_{13}<0$ axis mainly accesses the dephasing of the *X*-*X* coherence. Along the negative Δt_{12} axis, pulses $\mathbf{k}_1$ and $\mathbf{k}_3$ arrive first ($\Delta t_{13}=0$) and create a second-order *X*- or *Y*-state population, or a coherence between different *X* and *Y* states. These evolve and relax for a time interval $|\Delta t_{12}|$, at which time pulse $\mathbf{k}_2$ arrives. Therefore, the $\Delta t_{12}<0$ axis probes population relaxation and intraband coherence dephasing and oscillations. Finally, along the positive Δt_{12} axis, pulse $\mathbf{k}_2$ arrives first and creates an interband polarization, which evolves for a time interval Δt_{12} when pulses $\mathbf{k}_1$ and $\mathbf{k}_3$ arrive. Thus the $\Delta t_{12}>0$ axis mainly probes interband polarization dephasing. The dependence of the three-pulse FWM signal on the two time delays gives complementary information on the coherent and relaxation dynamics of the QHS.

The polarizations P_n, Eqs. (61)–(63), depend on the interactions V_{01}, Eq. (56), and $W_{\mathbf{q}n}$, Eq. (51). V_{01} gives static LL0-LL1 couplings and *X*-*X* interaction nonlinearities similar to the undoped system. $W_{\mathbf{q}n}\propto v_{01}^{01}(\mathbf{q})$ governs the *X*-2DEG scattering in the ideal QHS. Next we present numerical results that clarify the role of these two different interaction effects. Figure 4 shows the time evolution of the FWM signal at the LL0 and LL1 peak energies for photoexcitation triggered by optical pulses centered close to LL1 as in Fig. 3. Striking in Fig. 4 is that, despite the very different photoexcitation of the two LLs, the full calculation with $W_{\mathbf{q}n}\neq 0$ gives LL0 and LL1 FWM signals that are *comparable in magnitude* (solid line). This result is consistent with the experiments.[18,45–47] On the other hand, for $W_{\mathbf{q}n}=0$, $V_{01}\neq 0$, the LL0 signal is *much smaller* than the LL1 signal (dashed-dotted line in Fig. 4), as expected for LL1 photoexcitation and as observed experimentally in the undoped system.[50] We conclude that the *X*-2DEG interactions drastically enhance the LL0/LL1 FWM peak ratio. Figure 4 also shows that they

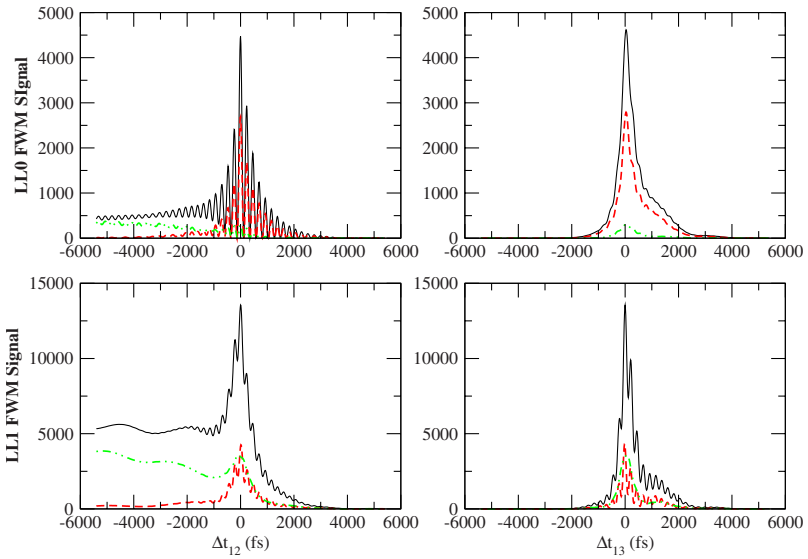

FIG. 5. (Color online) FWM contribution due to the PSF and X-X interaction nonlinearities [first three terms on the rhs of Eqs. (61) and (62)]. Solid line: $n_n=2P_n^LP_n^{L*}+2N_{nn}+\Sigma_{\mathbf{q}}\bar{n}_{\mathbf{q}}$. Dashed line: $n_n^X=2P_n^LP_n^{L*}+2N_{nn}$. Dashed-double dotted line: $n_n^Y=\Sigma_{\mathbf{q}}\bar{n}_{\mathbf{q}}$.

drastically change the decay and amplitude of the coherent FWM oscillations.

The X-2DEG interactions couple X_1 to the continuum of $Y_{\mathbf{q}}$ states, in a way that depends on the dispersion of their excitation energies $\bar{\Omega}_{\mathbf{q}}$. To study the effect of the MR minimum, which is characteristic of an incompressible quantum liquid, on the FWM signal, we compare in Fig. 4 [and in Fig. 7(a)] our full result to that obtained by treating the 2DEG interactions within the RPA (dashed line). The RPA dispersion broadens the LL1 FWM resonance while having a smaller effect on the LL0 FWM strength, a result consistent with the linear absorption behavior of Fig. 3. This RPA broadening is suppressed in the case of an incompressible quantum liquid and significantly depresses the LL1/LL0 FWM ratio. We thus conclude that the LL1/LL0 FWM peak ratio depends sensitively on the correlations leading to an incompressible quantum liquid with magnetoroton inter-LL excitations. The RPA also results in a faster decay of the LL0 coherent FWM oscillations along the $\Delta t_{12}<0$ axis. This oscillation decay is induced by the X-2DEG interaction. Importantly, the full calculation gives a nonexponential decay of the LL0 signal along the $\Delta t_{13}>0$ axis, absent within the RPA or for $W_{\mathbf{q}n}=0$. This behavior reflects the non-Markovian polarization dephasing due to X-Y coupling in the presence of MR excitations (compare the full and RPA calculations in Fig. 4 along the $\Delta t_{13}>0$ axis). We conclude that the temporal profile of the LL0 FWM signal in the case of LL1 photoexcitation may be used to measure the quantum dynamics due to magnetoexciton interactions with an incompressible 2DEG, which differs significantly as compared to the RPA.

The PSF and X-X interaction nonlinearities, previously studied for magnetoexcitons in undoped semiconductors,[50,59,60] are described by the first three terms on the rhs of Eqs. (61) and (62). Figure 5 shows the contribution of these nonlinearities, which have the form $d(t)n_n$ (PSF) and P_nn_m, P_nN_{01} (X-X interactions), to the FWM signal and also includes the effects of the linear P_n-$\bar{P}_{\mathbf{q}}$ coupling [first two terms on the rhs of Eq. (63)], which gives interaction-induced polarization dephasing similar to the linear response. The above nonlinearities give a large part of the overall FWM signal in the ideal QHS. However, their contribution differs from the full result, Fig. 4, at the LL1 energy. This difference comes from the light-induced changes in the X energies, inter-LL couplings, and dephasing described by the rest of the nonlinear terms on the rhs of Eqs. (61)–(63), which are generated by the X-2DEG interaction $v_{01}^{01}(\mathbf{q})$. The PSF and X-X interactions give a large LL1/LL0 FWM peak ratio, similar to the $W_{\mathbf{q}n}=0$ result in Fig. 4 and the undoped system.[50] The $W_{\mathbf{q}n}=0$, $V_{01}\neq 0$ FWM signal differs from that in Fig. 5 due to the changes in the population relaxation and the dephasing of the $X_0\leftrightarrow X_1$ coherence induced by the X-2DEG interactions.

Figure 5 also compares the PSF+X-X interaction nonlinear contribution for populations given by (i) $n_n=n_n^X+n_n^Y$ (full result), (ii) $n_n=n_n^X=2P_n^LP_n^{L*}+2N_{nn}$ (population of X_n states only), and (iii) $n_n=n_n^Y=\Sigma_{\mathbf{q}}\bar{n}_{\mathbf{q}}$ (population of the continuum of $Y_{\mathbf{q}}$ states). The excitonic contribution to the LLn population, n_n^X, gives a FWM signal that decays for $\Delta t_{12}<0$ and is relatively small. The strong effect of the X-2DEG interaction on this excitonic signal can be seen by comparing it to the $W_{\mathbf{q}n}=0$, $V_{01}\neq 0$ result in Fig. 4 (dashed-dotted line). Importantly, Fig. 5 demonstrates that the $\Delta t_{12}<0$ axis FWM signal reflects the gradual buildup of the Y-state populations n_n^Y, due to the $X\rightarrow Y$ scattering, and increases slowly with time. We conclude that the population of the Y-state continuum states plays an important role in determining the magnitude and temporal profile of the FWM signal due to PSF+X-X interactions in the QHS.

To elucidate the nonlinear response due to the X-2DEG interaction, we show in Fig. 6 the FWM results obtained by setting $V_{01}=0$ and compare them to the noninteracting system for optical pulses tuned as in Fig. 3. For $V_{01}=0$, the X-X interactions and static LL0-LL1 couplings vanish, which affects both the linear and nonlinear polarizations. The nonlinearities then result from PSF and X-2DEG interactions. The latter interactions introduce the nonlinear terms in the last two lines on the rhs of Eqs. (61) and (62) and on the rhs of Eq. (63). They also change the carrier relaxation, which affects the PSF contribution. We see in Fig. 6 that the LL0 FWM signal of the noninteracting system is very small, as expected for LL1 photoexcitation, and is determined by PSF

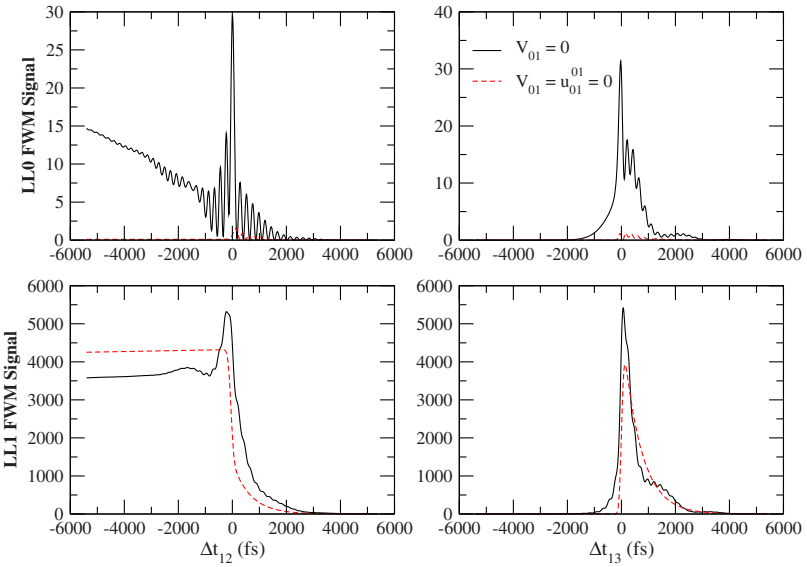

FIG. 6. (Color online) FWM signal for $V_{01}=0$. Solid line: effect of X-2DEG interactions, $W_{\mathbf{q}n}\neq 0$. Dashed line: noninteracting system, $W_{\mathbf{q}n}=0$.

alone. For $W_{\mathbf{q}n}\neq 0$, the X-2DEG interactions generate a LL0 signal that increases slowly with time along the LL0 $\Delta t_{12}<0$ axis, which reflects the population dynamics. However, this LL0 signal is still small in the case of LL1 photoexcitation of the ideal QHS as in Fig. 3. We thus conclude that the LL0 signal in Fig. 4 is mainly generated by X-X interactions modified by X-2DEG scattering. The nonlinearities generated by the X-2DEG interaction give the $\Delta t_{13}<0$ FWM signal in Fig. 6, which cannot arise from PSF, and lead to nonexponential decay along the $\Delta t_{13}>0$ axis. The overall FWM behavior results from the interplay between the X-X and X-Y interactions, whose relative contribution depends on the particularities of the realistic system.

Next we consider the coupling between the nonlinear coherences P_n and $\bar{P}_{\mathbf{q}}$ due to the X-2DEG interaction. As already seen by the emergence of the extra absorption peak in Fig. 3, the linear P_1^L-$\bar{P}_{\mathbf{q}}^L$ coupling changes drastically the 1-h eigenstates, in a way that depends critically on the dispersion of the $Y_{\mathbf{q}}$ states. The X and $Y_{\mathbf{q}}$ states are not eigenstates of the system, as demonstrated by the comparison to the results obtained for $W_{\mathbf{q}n}=0$, in which case X_n are approximate eigenstates in our calculation. Rather, the equations of motion, Eqs. (61)–(63), describe polaronic effects in the time domain that lead to eigenstates consisting of a coherent superposition of X_1 and $Y_{\mathbf{q}}$ configurations. Figure 7(b) shows the result obtained by only retaining the first two terms on the rhs of Eq. (63), which treats the above coupling similar to the linear polarization calculation. The comparison of Fig. 7(b) to the full calculation, Fig. 7(a), shows that the nonlinear contributions to $\bar{P}_{\mathbf{q}}$ mainly decrease the $\Delta t_{12}<0$ LL1 signal but do not change the overall qualitative behavior. Figure 7 also compares the full and RPA dispersion calculations and shows more clearly that the RPA dispersion depresses the LL1 nonlinear signal and enhances the decay of the LL0 coherent FWM oscillations. The RPA broadening comes from the X_1 coupling to the entire $Y_{\mathbf{q}}$ continuum, given by the first line on the rhs of Eq. (63), which is suppressed in the full calculation due to the MR excitation energy minimum of the incompressible quantum liquid.

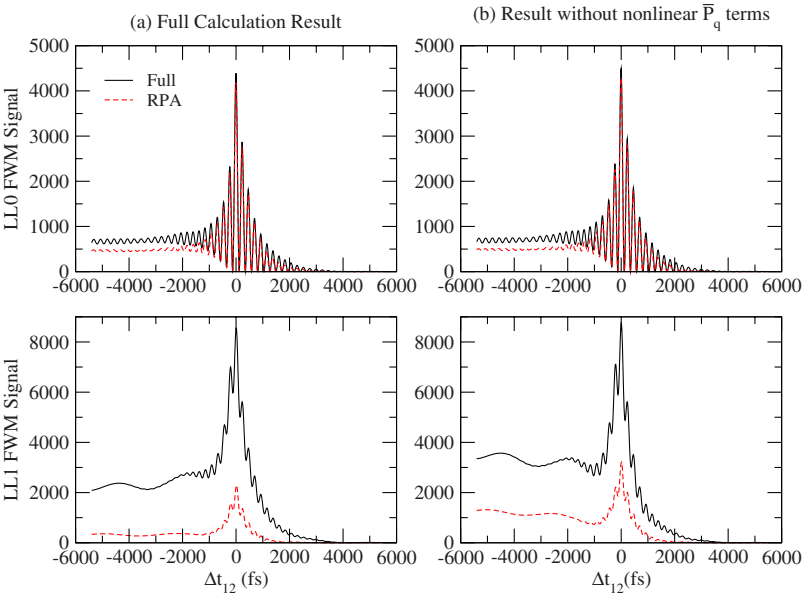

FIG. 7. (Color online) Effect of nonlinear contributions and 2DEG correlations on $\bar{P}_{\mathbf{q}}$. (a) Full calculation and (b) first two terms on the rhs of Eq. (63). Solid line: full dispersion $\bar{\Omega}_{\mathbf{q}}$. Dashed line: results using the RPA dispersion.

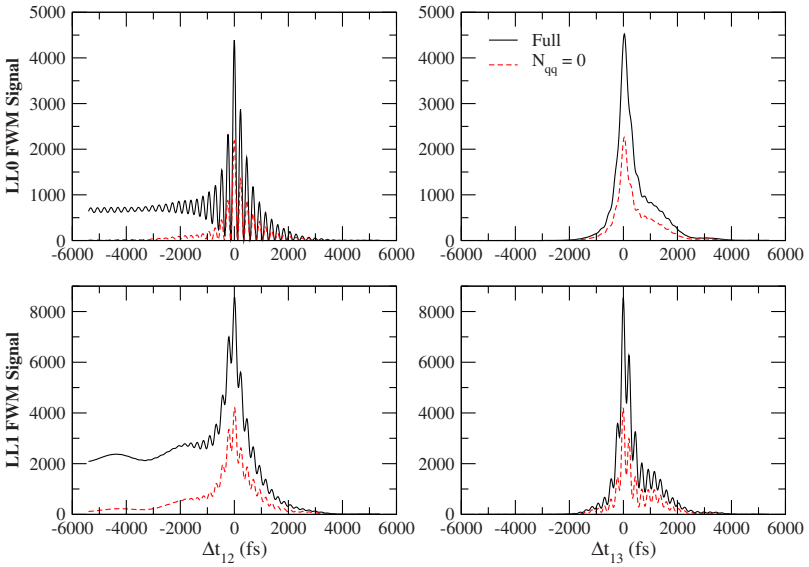

FIG. 8. (Color online) The role of the Y-state populations $N_{\mathbf{qq}}$. Solid line: full FWM calculation. Dashed line: FWM signal with $N_{\mathbf{qq}}=0$.

We now turn to the FWM signal generated by the Y-state populations $\bar{n}_{\mathbf{q}}(t)$, Eq. (66). In Fig. 8 we compare the full FWM calculation with the result obtained by setting $N_{\mathbf{qq}}=0$ in which case $\bar{n}_q=\bar{P}^{L*}_{\mathbf{q}}\bar{P}^{L}_{\mathbf{q}}$ is given by the Y-state coherences. Figure 8 demonstrates that the long-lived Y-state populations $N_{\mathbf{qq}}$ give a LL0 FWM signal that *rises* with $\Delta t_{12}<0$ following the initial coherent regime. This can be seen by comparing the full and $N_{\mathbf{qq}}=0$ results in Figs. 8(a) and 8(b). For $N_{\mathbf{qq}}=0$, the FWM signal decays fast along the $\Delta t_{12}<0$ axis. The full calculation signal builds up gradually and then decays as determined by the population relaxation rate $\Gamma_{pop}=\Gamma_{nn}=\Gamma_{\mathbf{qq}}$. This is seen more clearly in Figs. 9(a) and 9(b), where we compare the LL0 and LL1 FWM for the different relaxation rates given in the inset of Fig. 9(c). The rise time of the LL0 signal for $\Delta t_{12}<0$ reflects the slow buildup of $\bar{n}_{\mathbf{q}}(t)$, shown in Figs. 9(c) and 9(d) at different momenta, as the X states depopulate due to irreversible $X\rightarrow X+\mathrm{MP}$ scattering. Figure 9 shows that the dynamics of this X-2DEG interaction process can be resolved with femtosecond pulses. The strong coupling of the $X+\mathrm{MR}$ final states, missed by the RPA, is demonstrated by Fig. 9(d), which compares the populations of the $Y_{\mathbf{q}}$ states with $ql=2$ for the full or RPA dispersion. At such momenta, the two dispersions deviate strongly (see Fig. 2). Figure 9(d) shows that the MR excitations characteristic of the incompressible 2DEG result in larger $X+\mathrm{MR}$ populations as compared to the RPA, which implies stronger coupling of X_1 to the $Y_{\mathbf{q}}$ states with MR momenta.

The above results indicate the important role of carrier relaxation due to X-2DEG scattering on the three-pulse FWM signal, in addition to the non-Markovian polarization dephasing effects. Figures 10(a) and 10(b) show the time dependence of the total LLn carrier populations, n_n, for LL1 photoexcitation by a single pulse as in Fig. 3. The role of the X-2DEG interaction is seen by comparing to the populations obtained for $W_{\mathbf{q}n}=0$, $V_{01}\neq 0$ as in the undoped system. The LLn electron and hole populations, given by Eqs. (64) and (65), include coherent and incoherent contributions from both the X_n and $Y_{\mathbf{q}}$ states, which are shown in Figs. 10(c) and 10(d).

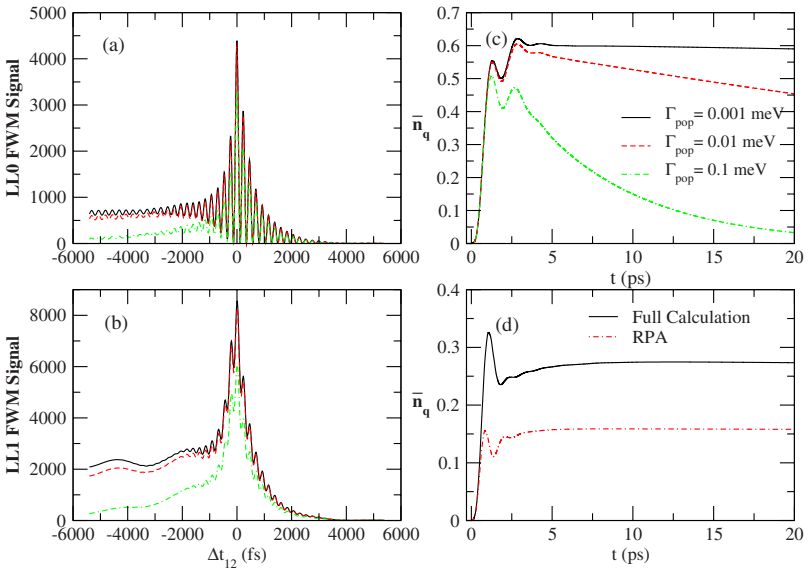

FIG. 9. (Color online) Dependence of the Δt_{12} axis FWM signal on the population relaxation rate $\Gamma_{pop}=\Gamma_{\mathbf{qq}}=\Gamma_{nn}$. (a) LL0 signal. (b) LL1 signal. (c) Time dependence of the Y-state population $\bar{n}_{\mathbf{q}}(t)$ for $ql=1$. (d) Comparison of $\bar{n}_{\mathbf{q}}(t)$ for $ql=2$ between full (solid line) and RPA (dashed-dotted line) Y-state dispersions.

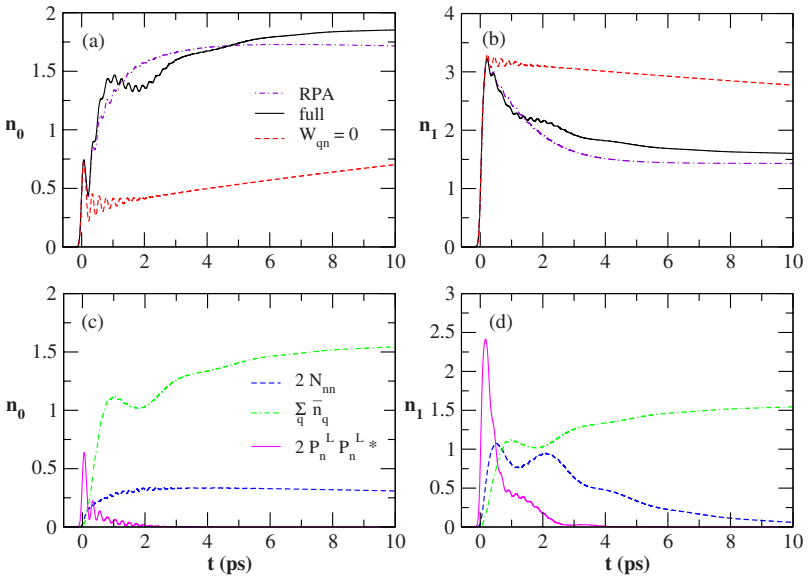

FIG. 10. (Color online) Time evolution of the total carrier populations $n_n(t)$. Solid line: full calculation. Dashed line: $W_{\mathbf{q}n}=0$, $V_{01}\neq 0$. Dashed-dotted line: RPA dispersion. [(c) and (d)] Coherent and incoherent contributions, Eqs. (64) and (65), to the LLn total electron and hole populations.

In the initial coherent temporal regime, $n_n \sim 2P_n^{L*}P_n^L$. The time evolution of these coherent exciton populations is shown in Figs. 10(c) and 10(d). The nonexponential time evolution of the LL1 populations in Fig. 10(d) is due to the emergence of the two LL1 peaks (Fig. 3) as a result of the MR dispersion minimum. By comparing to the RPA, Figs. 10(a) and 10(b) show that these quantum kinetic effects manifest themselves on the carrier relaxation. We also note that $n_1/n_0 \sim 4$ in the coherent regime due to the different photoexcitation of the two LLs. It is clear that the early time LL1/LL0 FWM ratio in Fig. 4 does not simply reflect the photoexcited carrier ratio n_1/n_0, in agreement with the experiment.[45,47]

Figures 10(a) and 10(b) clearly show that, following the initial coherent temporal regime, the X-2DEG interaction drastically changes the carrier relaxation and n_0/n_1 population ratio as compared to the undoped system. The LL0 population increases sharply for intermediate time scales [Fig. 10(a)] while simultaneously the LL1 population drops [Fig. 10(b)] and the Y-state populations build up [Figs. 9(c) and 9(d)]. The above dynamics is due to the $X_1 \rightarrow X_{01}+\mathrm{MP}$ interaction process of Fig. 1(a), which involves inter-LL 2DEG excitations and couples the two LLs. The population time dependence differs markedly for $W_{\mathbf{q}n}=0$ in which case the coupling of the X_0 and X_1 populations comes from the nonresonant e-h interaction process described by the $X_0 \leftrightarrow X_1$ coherence $N_{01}(t)$ in Eq. (34). In the QHS, the population relaxation is governed instead by the resonant $X_1 \rightarrow Y$ interactions and the $X_1 \leftrightarrow Y_{\mathbf{q}}$ coherence. The population time dependence becomes similar to the undoped system if we set $M_{n\mathbf{q}}=0$ in Eqs. (34) and (36). The LL0 population rise time in Fig. 10(a) is mainly determined by the dynamics of $M_{1\mathbf{q}}(t)$. At sufficiently long times, when the scattering is complete, the carrier populations n_n are determined by the total population of the continuum of $\{1\mathrm{MP}+1\text{-LL0-}e+1\text{-LL1-}h\}$ states, $n_n^Y=\Sigma_{\mathbf{q}}\bar{n}_{\mathbf{q}}$, whose time dependence and slow rise is shown in Figs. 10(c) and 10(d) (dashed-dotted line). As a result, $n_0 \sim n_1$ at long times, in contrast to the $W_{\mathbf{q}n}=0$ result, which gives $n_1 > n_0$ as in the undoped system.[50] Figures 10(c) and 10(d) also show the time dependence of the incoherent exciton populations $N_{nn}(t)$ (dashed line). N_{00} relaxes very slowly, as determined by Γ_{pop}. In contrast, the relaxation of N_{11} is fast in the QHS and occurs on a time scale of a few picoseconds, which coincides with the buildup of n_n^Y. This rapid relaxation of the LL1 excitonic population due to inter-LL MP scattering is absent for $W_{\mathbf{q}n}=0$ and changes the temporal profile of the 2DEG FWM.

VIII. CONCLUSIONS

In conclusion, we discussed in full detail a nonequilibrium many-body theory that describes the ultrafast coherent nonlinear optical response of magnetoexcitons interacting with an incompressible quantum liquid. For this, we developed a density-matrix quantum kinetic description of dephasing/decoherence and relaxation in systems with a strongly correlated ground state, which recovers established results in undoped semiconductors and does not adopt the semiclassical or Boltzmann pictures of instantaneous interactions, structureless 2DEG bath, and quasiequilibrium free energy.

Our main motivation for developing this theory was to identify the signatures of an incompressible quantum liquid in nonlinear optical spectroscopies and compare to recent experiments.[18,45–47] We note that photoexcitation with three time-delayed femtosecond optical pulses accesses a much larger phase space than the more conventional one-dimensional four-wave mixing or linear spectroscopic techniques. The main question down the road is how two-dimensional correlation spectroscopy[64] can be used to resolve the detailed dynamics of the fundamental many-body interaction processes in strongly correlated systems.

Our goal here was to identify generic temporal and spectral features due to exciton coupling with an incompressible quantum liquid. For this we presented numerical results obtained for an ideal two-dimensional 2DEG at filling factor $\nu=1$. This is the simplest system for studying the generic effects of inter-LL magnetoroton collective excitations, which are signatures of the many-body corrections in the

local field of an incompressible quantum liquid, and their coupling to X's. We studied the differences between the full calculation of the third-order nonlinear polarization and the results obtained by treating the 2DEG interactions within the RPA. The latter approximation only gives MP long-wavelength collective excitations but misses the magnetoroton minimum. We described the effects of the dynamical coupling between the X and X+MP or X+MR configurations by spectrally resolving the FWM signal and then comparing its strength and time evolution along two time axes at the LL0 and LL1 energies. We showed that it is useful for drawing conclusions to excite the system close to the LL1 energy so that the LL0/LL1 ratio of photoexcited carrier populations is kept small and the phase-space filling nonlinearities at the LL0 energy are suppressed. A noninteracting multilevel system calculation then predicts a correspondingly small ratio of LL0/LL1 FWM signals. This also holds true in the undoped system,[50] despite the coupling of the LL0 and LL1 magnetoexcitons by the exciton-exciton interaction nonlinearities. The experimental measurements in the 2DEG revealed comparable LL0 and LL1 FWM signals for $\nu<2$ even though the photoexcited LL1 carriers far exceeded the photoexcited LL0 carriers, in sharp contrast to an undoped quantum well system under the same photoexcitation conditions.[45–47] These experiments also revealed the emergence of a strong high-energy shoulder above the LL1 exciton peak for $\nu<2$, as empty LL0 states become available for LL1$\rightarrow$LL0 scattering.[47] Our calculations offer a possible microscopic explanation of these experimental features, which clearly distinguish the dynamics of magnetoexcitons interacting with a 2DEG at filling factors $\nu<2$ from that of magnetoexcitons in an undoped semiconductor system. Here we also predict the experimental signatures of an incompressible 2DEG.

By treating the full quantum kinetics of the coupling between the LL1 magnetoexciton and the continuum of {1-LL0-e+1-LL1-h+LL0$\rightarrow$LL1MP} configurations, we obtained a double-peak spectral line shape close to the LL1 energy. This double resonance is suppressed by the RPA treatment of the 2DEG interactions, which misses the magnetoroton excitations and simply broadens the LL1 excitonic resonance. Such broadening is suppressed in our full calculation, which indicates polaronic effects due to the coupling of MRs. The above result may explain the experimental observation, for $\nu<2$, of a strong high-energy shoulder right above the LL1 energy while at the same time the LL0 resonance remains Lorentzian.[47] This difference in resonance line-shape results from the suppression of the X_0-2DEG coupling.

Our calculations show that the ratio of the LL1 and LL0 FWM resonance strengths does not simply reflect the photoexcited carrier populations, as in an atomiclike noninteracting system, but depends on interaction-induced nonlinearities and couplings in the presence of an interacting 2DEG. By only including the X-X interactions, or in a completely noninteracting system, we obtain a LL1 peak FWM signal that far exceeds the LL0 peak signal. In contrast, the full calculation gives comparable FWM peaks, despite the different LL0 and LL1 photoexcitations. This result is consistent with the experimental observations[45–47] and comes from the gradual population of {1-LL0-e+1-LL1-h+LL0$\rightarrow$LL1MP} configurations in the many-body eigenstates and from their coherent dynamical coupling to the discrete X states. Our quantum kinetic calculation shows that femtosecond optical pulses can be used to resolve the details of this noninstantaneous interaction process, whose dynamics is described by the time evolution of the X- and $Y_{\mathbf{q}}$-state populations coupled by a $X\leftrightarrow Y_{\mathbf{q}}$ coherence.

The comparison between our full calculation and the RPA results show that the optical spectra and their time evolution are sensitive to the magnetoroton minimum in the excitation dispersion of an incompressible liquid. The latter changes the exciton coupling to the continuum of X+MP configurations. In particular, the RPA dispersion broadens the LL1 resonance while this broadening is suppressed in the full calculation. This drastic effect of the 2DEG correlations strongly affects the LL1/LL0 FWM peak ratio and reflects on the time evolution of the FWM line shape. Along the Δt_{13} axis, the incompressible quantum liquid gives a nonexponential FWM decay that reflects the non-Markovian interaction-induced exciton dephasing. Along the Δt_{12} axis, the incompressible quantum liquid determines the decay time of the LL0 coherent FWM oscillations. Another experimental signature is the rise time of the $\Delta t_{12}<0$ LL0 FWM signal, which is determined by the X-Y coupling described by the dynamics and dephasing of the $X\leftrightarrow Y$ coherences. A comparison to the experimental results of Refs. 45–47 will be presented elsewhere.

The numerical calculations discussed here did not explore the full phase-space accessible with two-dimensional correlation spectroscopy.[64] Nevertheless, they clearly show that these experiments can isolate the different physical processes and measure the details of the magnetoexciton coupling to an incompressible quantum liquid at different filling factors and ground states. In the realistic system, the relative magnitude of the different competing contributions also depend on the valence band structure, disorder, finite quantum well confinement, doping asymmetry, and dephasing rates, which are clearly important for a detailed description of the experiments. For example, here we did not address the formation of trion states and their nonlinear response, or quasiexcitons at fractional filling factors. Future experimental and theoretical studies promise to elucidate the dynamics of both spin and charge elementary excitations and their interactions in strongly correlated systems.

ACKNOWLEDGMENTS

This work was supported by the EU ITN program ICARUS and by the EU STREP program HYSWITCH. We are grateful to J. Tignon and S. Cundiff for very useful discussions, and especially to D. S. Chemla for inspiring our work.

APPENDIX A

In the Landau gauge, the interaction matrix elements $v^{ij}_{\alpha_1\alpha_2,\alpha_3\alpha_4}$ (with $i,j=e,h$) are given by

$$v^{ij}_{\alpha_1\alpha_2,\alpha_3\alpha_4} = \int \frac{d\mathbf{q}}{(2\pi)^2} v_q F^i_{\alpha_1\alpha_2}(\mathbf{q}) F^j_{\alpha_3\alpha_4}(-\mathbf{q}), \tag{A1}$$

where v_q is the Coulomb potential,

$$F^e_{\alpha_1\alpha_2}(\mathbf{q}) = \phi_{n_1 n_2}(\mathbf{q}) e^{iq_x(k_1+k_2)\ell^2/2} \delta_{k_1,k_2+q_y} \delta_{\sigma_1,\sigma_2} \tag{A2}$$

and

$$F^h_{\alpha_1\alpha_2}(\mathbf{q}) = F^e_{-\alpha_2,-\alpha_1}(\mathbf{q}), \quad -\alpha = (-k,n,\sigma). \tag{A3}$$

In the above equations,

$$\phi_{mn}(\mathbf{q}) = \frac{n!}{m!}\left[\frac{(-q_y + iq_x)l}{\sqrt{2}}\right]^{m-n} L_n^{m-n}\left(\frac{q^2\ell^2}{2}\right) e^{-q^2\ell^2/4} \tag{A4}$$

for $m \geq n$ and $\phi_{mn}(\mathbf{q}) = \phi^*_{nm}(-\mathbf{q})$ for $m < n$, where L_n^{m-n} is the generalized Laguerre polynomial.

APPENDIX B

The density-matrix equation of motion for a general operator $\hat{O}$ is given by

$$i\partial_t \langle \hat{O} \rangle = \langle [\hat{O}, H] \rangle - d(t)\sqrt{N}\sum_m \langle [\hat{O}, \hat{X}^\dagger_m] \rangle - d^*(t)\sqrt{N}\sum_m \langle [\hat{O}, \hat{X}_m] \rangle. \tag{B1}$$

The deviation from bosonic behavior of a LLn electron-LLm hole excitation is determined by the commutator

$$[\hat{X}_{\mathbf{q}nm}, \hat{X}^\dagger_{\mathbf{q}'n'm'}] = \delta_{\mathbf{q}\mathbf{q}'}\delta_{nn'}\delta_{mm'} - \frac{\hat{\rho}^h_{\mathbf{q}'-\mathbf{q},m'm\downarrow}}{\sqrt{N}}\delta_{nn'} e^{i(\mathbf{q}'\times\mathbf{q})_z l^2/2} - \frac{\hat{\rho}^e_{\mathbf{q}'-\mathbf{q},n'n\downarrow}}{\sqrt{N}}\delta_{mm'} e^{-i(\mathbf{q}'\times\mathbf{q})_z l^2/2}. \tag{B2}$$

The Pauli exchange effects between X's and 2DEG collective excitations, as well as between photoexcited carriers, are described by the commutators

$$[\hat{\rho}^e_{\mathbf{q}nm\sigma}, \hat{X}^\dagger_{\mathbf{q}'n'm'}] = \frac{1}{\sqrt{N}}\delta_{\sigma\downarrow}\delta_{mm'} e^{i(\mathbf{q}\times\mathbf{q}')_z\ell^2/2}\hat{X}^\dagger_{\mathbf{q}+\mathbf{q}'nm'} \tag{B3}$$

and

$$[\hat{\rho}^h_{\mathbf{q}nm\sigma}, \hat{X}^\dagger_{\mathbf{q}'n'm'}] = \frac{1}{\sqrt{N}}\delta_{\sigma\downarrow}\delta_{mm'} e^{-i(\mathbf{q}\times\mathbf{q}')_z\ell^2/2}\hat{X}^\dagger_{\mathbf{q}+\mathbf{q}'n'n}. \tag{B4}$$

Finally, the Pauli exchange effects between the 2DEG excitations, which distinguish the QHS from the undoped system, are described by the commutators

$$[\hat{\rho}^e_{\mathbf{q}nn'\sigma}, \hat{\rho}^e_{\mathbf{q}'mm'\sigma'}] = \frac{\delta_{\sigma\sigma'}\delta_{n'm}}{\sqrt{N}} e^{i(\mathbf{q}\times\mathbf{q}')_z\ell^2/2}\hat{\rho}^e_{\mathbf{q}+\mathbf{q}'nm'\sigma} - \frac{\delta_{\sigma\sigma'}\delta_{nm'}}{\sqrt{N}} e^{-i(\mathbf{q}\times\mathbf{q}')_z\ell^2/2}\hat{\rho}^e_{\mathbf{q}+\mathbf{q}'mn'\sigma}. \tag{B5}$$

APPENDIX C

In this appendix we present the commutators with the many-body Hamiltonian given by Eqs. (1) and (2), which describe the interaction contribution to the equation of motion Eq. (B1). For a general interband e-h excitation, we obtain after some straightforward algebra

$$[\hat{X}_{\mathbf{q}nm}, H] = [E_g + (n+1/2)\omega^e_c + (m+1/2)\omega^h_c]\hat{X}_{\mathbf{q}nm} - \sum_{n'm'} \bar{V}_{m'm,n'n}(\mathbf{q})\hat{X}_{\mathbf{q}n'm'} + \frac{1}{2\pi l^2\sqrt{N}}\sum_{\mathbf{q}'n'} v_{q'}\hat{\rho}_{-\mathbf{q}'}[\phi_{nn'}(\mathbf{q}')e^{-i(\mathbf{q}\times\mathbf{q}')_z l^2/2}\hat{X}_{\mathbf{q}-\mathbf{q}'n'm} - \phi_{n'm}(\mathbf{q}')e^{i(\mathbf{q}\times\mathbf{q}')_z l^2/2}\hat{X}_{\mathbf{q}-\mathbf{q}'nn'}]. \tag{C1}$$

In the QHS we must also consider the dynamics and interactions of the 2DEG collective excitation operators $\hat{\rho}^e_{\mathbf{q}mm'\sigma}$,

$$[\hat{\rho}^e_{\mathbf{q}nm\sigma}, H] = \left[\omega^e_c(m-n) + \sum_{n'} V_{n'n}\right]\hat{\rho}^e_{\mathbf{q}nm\sigma} - \sum_{n'm'} \bar{V}_{mm',nn'}(\mathbf{q})\hat{\rho}^e_{\mathbf{q}n'm'\sigma} + \frac{1}{2\pi\ell^2\sqrt{N}}\sum_{\mathbf{q}'n'} v_{q'}\hat{\rho}_{-\mathbf{q}'}[\phi_{mn'}(\mathbf{q}')\hat{\rho}^e_{\mathbf{q}+\mathbf{q}'nn'\sigma}e^{i(\mathbf{q}\times\mathbf{q}')_z\ell^2/2} - \phi_{n'n}(\mathbf{q}')\hat{\rho}^e_{\mathbf{q}+\mathbf{q}'n'm\sigma}e^{-i(\mathbf{q}\times\mathbf{q}')_z\ell^2/2}]. \tag{C2}$$

In the above equations we used the interaction matrix elements Eq. (56) and defined

$$\bar{V}_{nn',mm'}(\mathbf{q}) = \int \frac{d\mathbf{q}'}{(2\pi)^2} v_{q'} e^{i(\mathbf{q}\times\mathbf{q}')_z l^2} \phi_{nn'}(\mathbf{q}') \phi^*_{mm'}(\mathbf{q}'). \tag{C3}$$

Using the above equations and the $\nu=1$ ground state, we obtain the dispersion of the X_{01} excitation,

$$\Omega_{\mathbf{q}01} = E_g + \frac{\Omega^c_c}{2} + \frac{3\Omega^v_c}{2} - \bar{V}_{11,00}(\mathbf{q}) \tag{C4}$$

and the energy of the MP excitations,

$$\omega_{\mathbf{q}} = \Omega^c_c + V_{00} - V_{10} + v^{01}_{01}(\mathbf{q}) - \bar{V}_{11,00}(\mathbf{q}). \tag{C5}$$

APPENDIX D

In this appendix we express the intraband density matrices in Eq. (19) in terms of Hubbard operators at $\nu=1$ after restricting to the photoexcited (first two) LLs. First we consider the X-X density matrices $\langle \hat{X}^\dagger_{mn\mathbf{q}} \hat{X}_{m'n'\mathbf{q}} \rangle$. Using the commutator Eq. (B2), we obtain

$$\langle X_l | \hat{X}^\dagger_{mn\mathbf{q}} \hat{X}_{m'n'\mathbf{q}} | X_{l'} \rangle = \delta_{\mathbf{q}0} \delta_{m'n'} \delta_{mn} \delta_{ml} \delta_{m'l'}, \tag{D1}$$

$$\langle Y_{\mathbf{Q}} | \hat{X}^\dagger_{mn\mathbf{q}} \hat{X}_{m'n'\mathbf{q}} | Y_{\mathbf{Q}'} \rangle = \delta_{\mathbf{Q}'\mathbf{q}} \delta_{\mathbf{Q}\mathbf{q}} \delta_{m0} \delta_{n1} \delta_{m'0} \delta_{n'1} \tag{D2}$$

while $\langle X_l | \hat{X}^\dagger_{mn\mathbf{q}} \hat{X}_{m'n'\mathbf{q}} | Y_{\mathbf{Q}} \rangle = 0$. We thus obtain for the X populations and $X \leftrightarrow X$ coherences

$$\langle \hat{X}^\dagger_{mn\mathbf{q}} \hat{X}_{m'n'\mathbf{q}} \rangle = \delta_{\mathbf{q}0} \delta_{m'n'} \delta_{mn} \langle |X_m\rangle\langle X_{m'}| \rangle + \delta_{m0}\delta_{m'0}\delta_{n1}\delta_{n'1} \langle |Y_{\mathbf{q}}\rangle \times \langle Y_{\mathbf{q}}| \rangle, \tag{D3}$$

which differ from the undoped system due to the contribution of the Y states. Next we consider the density matrices of the form $\langle \hat{\rho}_\sigma \hat{\rho}_\downarrow \rangle$. Using the commutators [Eqs. (B2)–(B4) and (17)] we obtain the matrix elements

$$\langle X_{l'} | \hat{\rho}_{-\mathbf{q}} \hat{\rho}^e_{\mathbf{q}nm\downarrow} | X_l \rangle = \frac{\delta_{ml}}{N} [\phi^*_{nl}(\mathbf{q}) \delta_{ll'} - \phi^*_{l'l}(\mathbf{q}) \delta_{nl'}], \tag{D4}$$

$$\langle X_{l'} | \hat{\rho}_{-\mathbf{q}} \hat{\rho}^h_{\mathbf{q}nm\downarrow} | X_l \rangle = \frac{\delta_{ml}}{N} [\phi^*_{ll'}(\mathbf{q}) \delta_{nl'} - \phi^*_{ln}(\mathbf{q}) \delta_{ll'}]. \tag{D5}$$

The coupling between the X and Y states is described by the matrix elements

$$\langle Y_{\mathbf{Q}} | \hat{\rho}_{-\mathbf{q}} \hat{\rho}^e_{\mathbf{q}01\downarrow} | X_l \rangle = \frac{\phi^*_{01}(\mathbf{q})}{\sqrt{N}} \delta_{\mathbf{q}\mathbf{Q}} \delta_{l1}, \tag{D6}$$

$$\langle X_l | \hat{\rho}_{-\mathbf{q}} \hat{\rho}^e_{\mathbf{q}10\downarrow} | Y_{\mathbf{Q}} \rangle = \frac{\phi^*_{10}(\mathbf{q})}{\sqrt{N}} \delta_{\mathbf{q},-\mathbf{Q}} \delta_{l1}, \tag{D7}$$

$$\langle Y_{\mathbf{Q}} | \hat{\rho}_{-\mathbf{q}} \hat{\rho}^h_{\mathbf{q}10\downarrow} | X_l \rangle = \frac{\phi^*_{01}(\mathbf{q})}{\sqrt{N}} \delta_{\mathbf{q}\mathbf{Q}} \delta_{l0}, \tag{D8}$$

$$\langle X_l | \hat{\rho}_{-\mathbf{q}} \hat{\rho}^h_{\mathbf{q}01\downarrow} | Y_{\mathbf{Q}} \rangle = \frac{\phi^*_{10}(\mathbf{q})}{\sqrt{N}} \delta_{\mathbf{q},-\mathbf{Q}} \delta_{l0}, \tag{D9}$$

while $\langle Y|\hat{\rho}\hat{\rho}^e_{\mathbf{q}10\downarrow}|X\rangle = \langle Y|\hat{\rho}\hat{\rho}^h_{\mathbf{q}01\downarrow}|X\rangle = \langle X|\hat{\rho}\hat{\rho}^e_{\mathbf{q}01\downarrow}|Y\rangle = \langle X|\hat{\rho}\hat{\rho}^h_{\mathbf{q}10\downarrow}|Y\rangle = 0$. Finally, for $\mathbf{q} \neq 0$, we obtain that

$$\langle Y_{\mathbf{Q}'} | \hat{\rho}_{-\mathbf{q}} \hat{\rho}^e_{\mathbf{q}10\downarrow} | Y_{\mathbf{Q}} \rangle = \frac{\phi^*_{10}(\mathbf{q}) \delta_{\mathbf{Q}'\mathbf{Q}}}{N}, \tag{D10}$$

$$\langle Y_{\mathbf{Q}'} | \hat{\rho}_{-\mathbf{q}} \hat{\rho}^h_{\mathbf{q}01\downarrow} | Y_{\mathbf{Q}} \rangle = -\frac{\delta_{\mathbf{Q}\mathbf{Q}'}}{N} \phi^*_{10}(\mathbf{q}) \tag{D11}$$

while $\langle Y|\hat{\rho}\hat{\rho}^h_{10\downarrow}|Y\rangle = \langle Y|\hat{\rho}\hat{\rho}^e_{01\downarrow}|Y\rangle = 0$. Using the above matrix elements and Eq. (66), we obtain

$$\langle \hat{\rho}_{-\mathbf{q}} \hat{\rho}^e_{\mathbf{q}10\downarrow} \rangle_c = \phi^*_{10}(\mathbf{q}) \left(N_{00} - N_{10} + \sqrt{N} M_{1,-\mathbf{q}} + \sum_{\mathbf{q}'} \bar{n}_{\mathbf{q}'} \right), \tag{D12}$$

$$\langle \hat{\rho}_{-\mathbf{q}} \hat{\rho}^e_{\mathbf{q}01\downarrow} \rangle_c = \phi^*_{01}(\mathbf{q}) (N_{11} - N^*_{10} + \sqrt{N} M^*_{1\mathbf{q}}), \tag{D13}$$

$$\langle \hat{\rho}_{-\mathbf{q}} \hat{\rho}^h_{\mathbf{q}10\downarrow} \rangle_c = -\phi^*_{01}(\mathbf{q}) (N_{00} - N_{10} - \sqrt{N} M^*_{0\mathbf{q}}), \tag{D14}$$

$$\langle \hat{\rho}_{-\mathbf{q}} \hat{\rho}^h_{\mathbf{q}01\downarrow} \rangle_c = -\phi^*_{10}(\mathbf{q}) \left(N_{11} - N^*_{10} - \sqrt{N} M_{0,-\mathbf{q}} + \sum_{\mathbf{q}'} \bar{n}_{\mathbf{q}'} \right). \tag{D15}$$

The photoexcited electron and hole incoherent populations are obtained after expanding the operators [Eq. (6)] in terms of Hubbard operators,

$$\bar{\nu}^e_0 = N_{00} + \sum_q \bar{n}_{\mathbf{q}}, \quad \bar{\nu}^h_0 = N_{00} \tag{D16}$$

gives the LL0 electron and hole populations while

$$\bar{\nu}^e_1 = N_{11}, \quad \bar{\nu}^h_1 = N_{11} + \sum_{\mathbf{q}} \bar{n}_{\mathbf{q}} \tag{D17}$$

gives the LL1 carrier populations. The incoherent total carrier populations, $\bar{\nu}_n = \bar{\nu}^e_n + \bar{\nu}^h_n$, are then given by Eq. (65) while $\bar{\nu}^e_{10} = N_{10} = \bar{\nu}^h_{10}$. Substituting the above results into Eq. (19) we obtain the intraband interaction-induced density-matrix contribution to Eqs. (61) and (62).

APPENDIX E

In this appendix we derive the equation of motion for the correlated contribution $\bar{P}_{\mathbf{q}}$ to the nonlinear polarization equation of motion. At $\nu=1$, we note that

$$\hat{X}_n | Y_{\mathbf{q}} \rangle = 0 \tag{E1}$$

while $\langle Y_{\mathbf{q}} | \hat{\rho}_{01} | Y_{\mathbf{q}'} \rangle = 0$ since we restrict to states with up to one MP. Using the property $[\hat{Y}_{\mathbf{q}}, \hat{X}_n] = [\hat{Y}_{\mathbf{q}}, \hat{Y}_{\mathbf{q}'}] = 0$,

$$\bar{P}_{\mathbf{q}} = \frac{1}{\sqrt{N}}\langle\psi_0||G\rangle\langle Y_{\mathbf{q}}||\psi_1\rangle + \frac{1}{\sqrt{N}}\langle\bar{\psi}_0||G\rangle\langle Y_{\mathbf{q}}||\bar{\psi}_1\rangle + \sum_m P_m^{L*}\langle Y_{\mathbf{q}}\hat{X}_m|\psi_2\rangle + \frac{1}{\sqrt{N}}\sum_m \langle\bar{\psi}_1||X_m\rangle\langle Y_{\mathbf{q}}\hat{X}_m||\bar{\psi}_2\rangle + \frac{1}{\sqrt{N}}\sum_{\mathbf{q}'}\langle\bar{\psi}_1||Y_{\mathbf{q}'}\rangle\langle Y_{\mathbf{q}}Y_{\mathbf{q}'}||\bar{\psi}_2\rangle, \tag{E2}$$

where we introduced the Y-Y states $|Y_{\mathbf{q}}Y_{\mathbf{q}'}\rangle = \hat{Y}_{\mathbf{q}}^{\dagger}\hat{Y}_{\mathbf{q}'}^{\dagger}|G\rangle$. An analogous expression can be obtained for the nonlinear polarization P_n by substituting $\hat{Z}=X_n$ in Eq. (44). Noting from Eqs. (5) and (46) that

$$\sum_m P_m^L\langle\bar{\psi}_{1L}|[\hat{X}_n,\hat{X}_m^{\dagger}]|\bar{\psi}_{1L}\rangle = -P_n^L\bar{\nu}_n + P_n^L\langle\bar{\psi}_{1L}|\bar{\psi}_{1L}\rangle \tag{E3}$$

and using Eq. (E1),

$$P_n = \frac{1}{\sqrt{N}}\langle\psi_0|G\rangle\langle X_n|\psi_1\rangle + \frac{1}{\sqrt{N}}\langle\bar{\psi}_0||G\rangle\langle X_n||\bar{\psi}_1\rangle + \sum_m P_m^{L*}\langle X_m X_n|\psi_2\rangle + \frac{1}{\sqrt{N}}\sum_m \langle\bar{\psi}_1||X_m\rangle\langle X_n X_m||\bar{\psi}_2\rangle + \frac{1}{\sqrt{N}}\sum_{\mathbf{q}'}\langle\bar{\psi}_1||Y_{\mathbf{q}'}\rangle\langle Y_{\mathbf{q}'}X_n||\bar{\psi}_2\rangle + P_n^L\langle\bar{\psi}_{1L}|\bar{\psi}_{1L}\rangle - P_n^L\bar{\nu}_n. \tag{E4}$$

We obtain the equation of motion of $\bar{P}_{\mathbf{q}}$ from Eq. (E2) after noting that the time evolution of the correlated 2-h state, obtained from Eq. (40), is given by Eq. (41).[15,17] Similarly,[15,17]

$$i\partial_t|\bar{\psi}_0\rangle = H|\bar{\psi}_0\rangle - \sum_n \langle\hat{Y}_n\rangle^{L*}\hat{X}_n|\bar{\psi}_{1L}\rangle + \sum_n \langle\hat{X}_n\rangle^{L*}[\hat{Y}_n|\bar{\psi}_{1L}\rangle - \langle\hat{Y}_n\rangle^L|G\rangle], \tag{E5}$$

where we used Eq. (E1) and[15,17]

$$i\partial_t|\bar{\psi}_{1L}\rangle = H|\bar{\psi}_{1L}\rangle + \sum_n \langle\hat{X}_n\rangle^L|Y_n\rangle - \sum_{n\mathbf{q}} W_{n\mathbf{q}}\bar{P}_{\mathbf{q}}^L|X_n\rangle. \tag{E6}$$

Using Eqs. (B1), (11), and (27), Eq. (5), the properties $H|G\rangle=0$ and

$$\hat{\nu}_n|Y_{\mathbf{q}}\rangle = \frac{1}{N}|Y_{\mathbf{q}}\rangle, \tag{E7}$$

Equations (31)–(33), Eq. (40), the orthogonality

$$\langle Y_{\mathbf{q}}Y_{\mathbf{q}'}|X_nX_m\rangle = \langle Y_{\mathbf{q}}Y_{\mathbf{q}'}|X_nY_{q''}\rangle = \langle X_nY_q|X_{n'},X_{m'}\rangle = 0 \tag{E8}$$

and Eq. (28), we obtain after some algebra the equation of motion (exact at $\nu=1$ within our subspace)

$$\begin{aligned} i\partial_t\bar{P}_{\mathbf{q}} = {} & (\bar{\Omega}_{\mathbf{q}} - i\gamma)\bar{P}_{\mathbf{q}} + \frac{1}{N}\sum_{\mathbf{q}'} W_{\mathbf{q}\mathbf{q}'}\bar{P}_{\mathbf{q}'} + \frac{1}{\sqrt{N}}\sum_n W_{\mathbf{q}n}P_n + d(t)\sum_n P_n^{L*}\bar{P}_{\mathbf{q}}^L + \frac{1}{\sqrt{N}}\sum_n W_{\mathbf{q}n}P_n^L\bar{\nu}_n + \frac{1}{\sqrt{N}}\sum_{n\mathbf{q}'} W_{\mathbf{q}'n}P_n^L\bar{P}_{\mathbf{q}'}^{L*}\bar{P}_{\mathbf{q}}^L \\ & + \sum_{nmm'} P_n^L\left[P_m^{L*}P_{m'}^L\frac{N}{2}\langle G|[\hat{Y}_{\mathbf{q}},\hat{Y}_m]|X_nX_{m'}\rangle + N_{mm'}N\langle X_m|\Delta[\hat{Y}_{\mathbf{q}}\hat{Y}_n^{\dagger}]X_{m'}\rangle\right] + \sum_{nn'\mathbf{q}'} P_n^L[P_{n'}^{L*}\bar{P}_{\mathbf{q}'}^L N\langle G|[\hat{Y}_{\mathbf{q}},\hat{Y}_{n'}]|X_nY_{\mathbf{q}'}\rangle \\ & + M_{n'\mathbf{q}'}N\langle X_{n'}\hat{Y}_{\mathbf{q}}|[\hat{Y}_n^{\dagger},\hat{Y}_{\mathbf{q}'}^{\dagger}]|G\rangle] + \sum_{n\mathbf{q}'\mathbf{q}''} P_n^L\bar{n}_{\mathbf{q}'\mathbf{q}''}N[\langle Y_{\mathbf{q}'}|\Delta[\hat{Y}_{\mathbf{q}}\hat{Y}_n^{\dagger}]|Y_{\mathbf{q}''}\rangle - \delta_{\mathbf{q}''\mathbf{q}}\langle Y_{\mathbf{q}'}|Y_n\rangle] + \frac{1}{\sqrt{N}}\sum_{nn'\mathbf{q}'} W_{n\mathbf{q}'}\bar{P}_{\mathbf{q}'}^L M_{n'\mathbf{q}}N[\delta_{nn'} \\ & - \langle X_{n'}Y_{\mathbf{q}}|X_nY_{\mathbf{q}}\rangle] + \sum_n P_n^{L*}\langle G|[\hat{Y}_{\mathbf{q}},\hat{Y}_n]|\bar{\psi}_2\rangle + \sum_{\mathbf{q}'}\bar{P}_{\mathbf{q}'}^{L*}\langle G|[\hat{Y}_{\mathbf{q}'},[\hat{Y}_{\mathbf{q}},H]]|\bar{\psi}_2\rangle. \end{aligned} \tag{E9}$$

The following interaction matrix elements are obtained after straightforward algebra at $\nu=1$ by using the commutators Eqs. (B3)–(B5) and the definition of the Y operators, Eqs. (49) and (50),

$$N\langle G|[\hat{Y}_{\mathbf{q}},\hat{Y}]|X_nX_m\rangle = \frac{v_{01}^{01}(q)}{\sqrt{N}}\times(\delta_{n1}\delta_{m0}+\delta_{n0}\delta_{m1}), \tag{E10}$$

$$N\langle X_m|\Delta[\hat{Y}_{\mathbf{q}}\hat{Y}^{\dagger}]|X_{m'}\rangle = -\frac{v_{01}^{01}(q)}{\sqrt{N}}\delta_{mm'} \tag{E11}$$

describe X-X interactions mediated by the emission and reabsorption of a MP,

$$N\langle G|[\hat{Y}_{\mathbf{q}},\hat{Y}]|X_nY_{\mathbf{q}'}\rangle = \delta_{\mathbf{q}\mathbf{q}'}(\delta_{n1}-\delta_{n0})[v_{01}^{01}(q)-V_{01}], \tag{E12}$$

$$N\langle X_nY_{\mathbf{q}}|X_{n'}Y_{\mathbf{q}'}\rangle = \delta_{nn'}\delta_{\mathbf{q}\mathbf{q}'}(N-1) \tag{E13}$$

describe X-Y interactions while

$$\langle Y_{\mathbf{q}}Y_{\mathbf{q}'}|Y_{\mathbf{q}''}Y_{\mathbf{q}'''}\rangle = \left\{\delta_{\mathbf{q}\mathbf{q}'''}\delta_{\mathbf{q}'\mathbf{q}''} + \delta_{\mathbf{q}\mathbf{q}''}\delta_{\mathbf{q}'\mathbf{q}'''} - \frac{2}{N}\delta_{\mathbf{q}+\mathbf{q}',\mathbf{q}''+\mathbf{q}'''}\cos\times\left[\frac{l^2}{2}(\mathbf{q}\times\mathbf{q}'+\mathbf{q}'\times\mathbf{q}''-\mathbf{q}\times\mathbf{q}'')_z\right]\right\}^2 \tag{E14}$$

describes Y-Y interactions. Using the above results and Eq. (51), we obtain from Eq. (E9) the equation of motion, Eq. (63), after neglecting the correlated 2-h contributions described by the amplitudes of $|\bar{\psi}_2\rangle$.

*Present address: Department of Physics, University of Konstanz, D-78464 Konstanz, Germany.

[1] D. S. Chemla and J. Shah, Nature (London) **411**, 549 (2001); D. S. Chemla, in *Non-linear Optics in Semiconductors*, edited by R. K. Willardson and A. C. Beers (Academic Press, New York, 1999).

[2] V. M. Axt and S. Mukamel, Rev. Mod. Phys. **70**, 145 (1998).

[3] F. Rossi and T. Kuhn, Rev. Mod. Phys. **74**, 895 (2002).

[4] W. Schäfer and M. Wegener, *Semiconductor Optics and Transport Phenomena* (Springer, New York, 2002).

[5] S. Das Sarma, M. Freedman, and C. Nayak, Phys. Rev. Lett. **94**, 166802 (2005).

[6] J. Shah, *Ultrafast Spectroscopy of Semiconductors and Semiconductor Nanostructures*, Springer Series in Solid-State Sciences Vol. 115, 2nd ed. (Springer-Verlag, Berlin, New York, 1999).

[7] H. Haug and S. W. Koch, *Quantum Theory of the Optical and Electronic Properties of Semiconductors* (World Scientific, Singapore, 1993).

[8] V. M. Axt, and A. Stahl, Z. Phys. B: Condens. Matter **93**, 195 (1994); K. Victor, V. M. Axt, and A. Stahl, Phys. Rev. B **51**, 14164 (1995).

[9] V. M. Axt, K. Victor, and A. Stahl, Phys. Rev. B **53**, 7244 (1996).

[10] I. E. Perakis and T. V. Shahbazyan, Surf. Sci. Rep. **40**, 1 (2000); Int. J. Mod. Phys. B **13**, 869 (1999); I. E. Perakis, Chem. Phys. **210**, 259 (1996).

[11] P. Kner, S. Bar-Ad, M. V. Marquezini, D. S. Chemla, and W. Schäfer, Phys. Rev. Lett. **78**, 1319 (1997); P. Kner, W. Schäfer, R. Lovenich, and D. S. Chemla, *ibid.* **81**, 5386 (1998).

[12] L. J. Sham, Phys. Rev. **150**, 720 (1966).

[13] I. Brener, W. H. Knox, and W. Schäefer, Phys. Rev. B **51**, 2005 (1995).

[14] I. E. Perakis and D. S. Chemla, Phys. Rev. Lett. **72**, 3202 (1994); T. V. Shahbazyan, N. Primozich, I. E. Perakis, and D. S. Chemla, *ibid.* **84**, 2006 (2000); N. Primozich, T. V. Shahbazyan, I. E. Perakis, and D. S. Chemla, Phys. Rev. B **61**, 2041 (2000).

[15] A. T. Karathanos, I. E. Perakis, N. A. Fromer, and D. S. Chemla, Phys. Rev. B **67**, 035316 (2003).

[16] I. E. Perakis and D. S. Chemla, Phys. Status Solidi B **234**, 242 (2002); I. E. Perakis, *ibid.* **238**, 502 (2003); I. E. Perakis and D. S. Chemla, Solid State Commun. **127**, 147 (2003).

[17] I. E. Perakis and E. G. Kavousanaki, Chem. Phys. **318**, 118 (2005).

[18] K. M. Dani, E. G. Kavousanaki, J. Tignon, D. S. Chemla, and I. E. Perakis, Solid State Commun. **140**, 72 (2006).

[19] E. G. Kavousanaki, K. M. Dani, J. Tignon, D. S. Chemla, and I. E. Perakis, Phys. Status Solidi B **243**, 2397 (2006).

[20] T. Chakraborty and P. Pietilainen, *The Quantum Hall Effects, Fractional and Integral*, 2nd ed. (Springer, New York, 1995).

[21] R. B. Laughlin, Phys. Rev. Lett. **50**, 1395 (1983).

[22] D. Yoshioka, *The Quantum Hall Effect*, Springer Series in Solid-State Sciences Vol. 133 (Springer-Verlag, Berlin, New York, 2002).

[23] A. Pinczuk, *Perspectives in Quantum Hall Effects: Novel Quantum Liquids in Low-Dimensional Semiconductor Structures* (Wiley, New York, 1996), Chap. 8.

[24] A. Pinczuk, J. P. Valladares, D. Heiman, A. C. Gossard, J. H. English, C. W. Tu, L. Pfeiffer, and K. West, Phys. Rev. Lett. **61**, 2701 (1988); A. Pinczuk, B. S. Dennis, L. N. Pfeiffer, and K. West, *ibid.* **70**, 3983 (1993); M. A. Eriksson, A. Pinczuk, B. S. Dennis, S. H. Simon, L. N. Pfeiffer, and K. W. West, *ibid.* **82**, 2163 (1999).

[25] C. Kallin and B. I. Halperin, Phys. Rev. B **30**, 5655 (1984).

[26] S. M. Girvin, A. H. MacDonald, and P. M. Platzman, Phys. Rev. Lett. **54**, 581 (1985).

[27] A. H. MacDonald, H. C. A. Oji, and S. M. Girvin, Phys. Rev. Lett. **55**, 2208 (1985); H. C. A. Oji and A. H. MacDonald, Phys. Rev. B **33**, 3810 (1986); A. H. MacDonald, J. Phys. C **18**, 1003 (1985).

[28] R. K. Kamilla, X. G. Wu, and J. K. Jain, Phys. Rev. B **54**, 4873 (1996).

[29] J. K. Jain, Phys. Rev. Lett. **63**, 199 (1989); Phys. Today **53**(4), 39 (2000).

[30] H. L. Stormer, D. C. Tsui, and A. C. Gossard, Rev. Mod. Phys. **71**, S298 (1999).

[31] A. Wójs, A. Gladysiewicz, and J. J. Quinn, Phys. Rev. B **73**, 235338 (2006); M. Byszewski, B. Chwalisz, D. K. Maude, M. L. Sadowski, M. Potemski, T. Saku, Y. Hirayama, S. Studenikin, D. G. Austing, A. S. Sachrajda, and P. Hawrylak, Nat. Phys. **2**, 239 (2006).

[32] S. M. Girvin and A. H. MacDonald, in *Novel Quantum Liquids in Low-Dimensional Semiconductor Structures*, edited by S. Das Sarma and A. Pinczuk (Wiley, New York, 1996).

[33] E. H. Rezayi, Phys. Rev. B **36**, 5454 (1987); **43**, 5944 (1991).

[34] S. L. Sondhi, A. Karlhede, S. A. Kivelson, and E. H. Rezayi, Phys. Rev. B **47**, 16419 (1993).

[35] A. H. MacDonald, H. A. Fertig, and L. Brey, Phys. Rev. Lett. **76**, 2153 (1996); H. A. Fertig, L. Brey, R. Côté, and A. H. MacDonald, Phys. Rev. B **50**, 11018 (1994); H. A. Fertig, L. Brey, R. Côté, A. H. MacDonald, A. Karlhede, and S. L. Sondhi, *ibid.* **55**, 10671 (1997).

[36] S. E. Barrett, G. Dabbagh, L. N. Pfeiffer, K. W. West, and R. Tycko, Phys. Rev. Lett. **74**, 5112 (1995); R. Tycko, S. E. Barrett, G. Dabbagh, L. N. Pfeiffer, and K. W. West, Science **268**, 1460 (1995).

[37] J. Sinova, A. H. MacDonald, and S. M. Girvin, Phys. Rev. B **62**, 13579 (2000).

[38] D. Heiman, B. B. Goldberg, A. Pinczuk, C. W. Tu, A. C. Gossard, and J. H. English, Phys. Rev. Lett. **61**, 605 (1988); B. B. Goldberg, D. Heiman, A. Pinczuk, L. N. Pfeiffer, and K. West, *ibid.* **65**, 641 (1990); A. J. Turberfield, S. R. Haynes, P. A. Wright, R. A. Ford, R. G. Clark, J. F. Ryan, J. J. Harris, and C. T. Foxon, *ibid.* **65**, 637 (1990).

[39] K.-B. Broocks, B. Su, P. Schröter, Ch. Heyn, D. Heitmann, W. Wegscheider, V. M. Apalkov, T. Chakraborty, I. E. Perakis, and C. Schüller, Phys. Status Solidi B **245**, 321 (2008).

[40] J. G. Groshaus, V. Umansky, H. Shtrikman, Y. Levinson, and I. Bar-Joseph, Phys. Rev. Lett. **93**, 096802 (2004); G. Yusa, H. Shtrikman, and I. Bar-Joseph, *ibid.* **87**, 216402 (2001).

[41] D. R. Yakovlev, V. P. Kochereshko, R. A. Suris, H. Schenk, W. Ossau, A. Waag, G. Landwehr, P. C. M. Christianen, and J. C. Maan, Phys. Rev. Lett. **79**, 3974 (1997).

[42] C. Schüller, K.-B. Broocks, Ch. Heyn, and D. Heitmann, Phys. Rev. B **65**, 081301(R) (2002).

[43] A. Wójs, J. J. Quinn, and P. Hawrylak, Phys. Rev. B **62**, 4630 (2000); A. Gładysiewicz, L. Bryja, A. Wójs, and P. Marek, *ibid.* **74**, 115332 (2006).

[44] N. A. Fromer, C. Schüller, D. S. Chemla, T. V. Shahbazyan, I. E. Perakis, K. Maranowski, and A. C. Gossard, Phys. Rev. Lett. **83**, 4646 (1999).

[45] N. A. Fromer, C. E. Lai, D. S. Chemla, I. E. Perakis, D. Driscoll, and A. C. Gossard, Phys. Rev. Lett. **89**, 067401 (2002).
[46] K. M. Dani, J. Tignon, M. Breit, D. S. Chemla, E. G. Kavousanaki, and I. E. Perakis, Phys. Rev. Lett. **97**, 057401 (2006).
[47] N. A. Fromer, C. Schüller, C. W. Lai, D. S. Chemla, I. E. Perakis, D. Driscoll, and A. C. Gossard, Phys. Rev. B **66**, 205314 (2002).
[48] C. Schüller, I. E. Perakis, N. A. Fromer, and D. S. Chemla, in *Nonequilibrium Physics at Short Time Scales: Formation of Correlations*, edited by K. Morawetz (Springer Verlag, Berlin, New York, 2004), p. 209.
[49] K. M. Dani, J. Tignon, M. Breit, D. S. Chemla, E. G. Kavousanaki, and I. E. Perakis, Physica E **34**, 206 (2006).
[50] K. M. Dani, I. A. Cotoros, J. Wang, J. Tignon, D. S. Chemla, E. G. Kavousanaki, and I. E. Perakis, Phys. Rev. B **78**, 041301(R) (2008).
[51] A. E. Ruckenstein and S. Schmitt-Rink, Int. J. Mod. Phys. B **3**, 1809 (1989); J. Igarashi, J. Phys. Soc. Jpn. **52**, 2827 (1983); **54**, 260 (1985); J. Igarashi, M. Takahashi, and T. Nagao, *ibid.* **68**, 3682 (1999).
[52] M. D. Kapetanakis and I. E. Perakis, Phys. Rev. B **78**, 155110 (2008); **75**, 140401(R) (2007); M. D. Kapetanakis, A. Manousaki, and I. E. Perakis, *ibid.* **73**, 174424 (2006); M. D. Kapetanakis and I. E. Perakis, Phys. Rev. Lett. **101**, 097201 (2008).
[53] T. Östreich, K. Schönhammer, and L. J. Sham, Phys. Rev. Lett. **74**, 4698 (1995); Phys. Rev. B **58**, 12920 (1998).
[54] E. Feenberg, *Theory of Quantum Fluids* (Academic Press, New York, 1969).
[55] A. B. Dzyubenko and A. Yu. Sivachenko, Phys. Rev. Lett. **84**, 4429 (2000); A. B. Dzyubenko, Phys. Rev. B **69**, 115332 (2004).
[56] I. V. Lerner and Yu. E. Lozovik, Zh. Eksp. Teor. Fiz. **80**, 1488 (1981) [Sov. Phys. JETP **53**, 763 (1981)]; A. H. MacDonald and E. H. Rezayi, Phys. Rev. B **42**, 3224 (1990).
[57] V. M. Apalkov and E. I. Rashba, Phys. Rev. B **46**, 1628 (1992); **48**, 18312 (1993).
[58] T. J. Park and J. C. Light, J. Chem. Phys. **85**, 5870 (1986).
[59] C. Stafford, S. Schmitt-Rink, and W. Schaefer, Phys. Rev. B **41**, 10000 (1990).
[60] T. V. Shahbazyan, N. Primozich, and I. E. Perakis, Phys. Rev. B **62**, 15925 (2000).
[61] N. R. Cooper and D. B. Chklovskii, Phys. Rev. B **55**, 2436 (1997).
[62] A. Wójs, I. Szlufarska, K.-S. Yi, and J. J. Quinn, Phys. Rev. B **60**, R11273 (1999).
[63] E. H. Aifer, B. B. Goldberg, and D. A. Broido, Phys. Rev. Lett. **76**, 680 (1996).
[64] L. Yang and S. Mukamel, Phys. Rev. Lett. **100**, 057402 (2008); L. Yang, T. Zhang, A. D. Bristow, S. T. Cundiff, and S. Mukamel, J. Chem. Phys. **129**, 234711 (2008); L. Yang, I. V. Schweigert, S. T. Cundiff, and S. Mukamel, Phys. Rev. B **75**, 125302 (2007).